CNWRA 98-004

EFFECT OF GALVANIC COUPLING BETWEEN OVERPACK MATERIALS OF HIGH-LEVEL NUCLEAR WASTE CONTAINERS – EXPERIMENTAL AND MODELING RESULTS

Prepared for

Nuclear Regulatory Commission
Contract NRC-02-97-009

Prepared by

Center for Nuclear Waste Regulatory Analyses
San Antonio, Texas

March 1998

CNWRA 98-004

EFFECT OF GALVANIC COUPLING BETWEEN OVERPACK MATERIALS OF HIGH-LEVEL NUCLEAR WASTE CONTAINERS – EXPERIMENTAL AND MODELING RESULTS

Prepared for

Nuclear Regulatory Commission
Contract NRC-02-97-009

Prepared by

Center for Nuclear Waste Regulatory Analyses
San Antonio, Texas

March 1998

CNWRA 98-004

EFFECT OF GALVANIC COUPLING BETWEEN OVERPACK MATERIALS OF HIGH-LEVEL NUCLEAR WASTE CONTAINERS— EXPERIMENTAL AND MODELING RESULTS

Prepared for

Nuclear Regulatory Commission
Contract NRC-02-97-009

Prepared by

Darrell S. Dunn
Gustavo A. Cragnolino

Center for Nuclear Waste Regulatory Analyses
San Antonio, Texas

March 1998

ABSTRACT

The effect of environmental parameters and area ratio on the galvanic protection of alloy 825 by A516 steel was studied. A simplified model was used to calculate the potential and corrosion current density of the bimetallic couple as a function of the galvanic coupling efficiency. Galvanic corrosion tests were performed to gain confidence in the calculated values. Both the calculations and laboratory testing indicate that the potential of the galvanic couple is maintained below the repassivation potential for alloy 825 in chloride-containing solutions if coupling is highly efficient. As a result, under conditions of efficient coupling, the initiation of localized corrosion on alloy 825 is prevented. The formation of oxides, scales, and corrosion product layers between the two materials is shown to reduce the efficiency of the galvanic coupling, however, the alloy 825 inner barrier will be galvanically protected from localized corrosion until the outer carbon steel overpack is consumed.

Keywords: Galvanic corrosion, high-level nuclear waste, localized corrosion, pitting corrosion, crevice corrosion, alloy 825, A516 steel.

CONTENTS

FIGURES

FIGURES (Cont'd)

TABLES

ACKNOWLEDGMENTS

This paper was prepared to document work performed by the Center for Nuclear Waste Regulatory Analyses (CNWRA) for the Nuclear Regulatory Commission (NRC) under Contract No. NRC-02-97-009. The activities reported here were performed on behalf of the NRC Office of Nuclear Material Safety and Safeguards Division of Waste Management. The report is an independent product of the CNWRA and does not necessarily reflect the views or regulatory position of the NRC.

The authors gratefully acknowledge the assistance of W. Machowski in conducting some of the experiments, the technical review of N. Sridhar, the programmatic review of B. Sagar, and the editorial review of C. Gray. Appreciation is due to J. Gonzalez for her assistance in the preparation of this report.

QUALITY OF DATA, ANALYSES, AND CODE DEVELOPMENT

DATA: CNWRA-generated original data contained in this paper meet quality assurance requirements described in the CNWRA Quality Assurance Manual. Sources for other data should be consulted for determining the level of quality for those data.

ANALYSES AND CODES: *Mathematica* Version 2.2.3, a commercial scientific software, was used for analyses contained in this report.

EXECUTIVE SUMMARY

The U.S. Department of Energy (DOE) updated strategy for radioactive waste containment and isolation for the proposed repository at the Yucca Mountain (YM) site is focused on two objectives: (i) to ensure near-complete containment of radionuclides within the waste packages (WPs) for thousands of years and (ii) to limit the dose to any member of the public throughout the compliance period. To accomplish these objectives, the proposed repository will be located in an arid site with a low annual precipitation rate and a low flow of groundwater into the repository horizon. In addition, the DOE has redesigned the WPs applying a double metallic barrier concept in an attempt to prolong the time during which the radioactive waste can be contained. In the current design, a corrosion allowance material (a carbon steel is the primary candidate) intended to corrode uniformly at a slow and predictable rate, constitutes the outer barrier. In the event the outer barrier is breached by pits, galvanic coupling of the inner corrosion resistant barrier (a Ni-base alloy) to the outer barrier is assumed to prevent pitting corrosion of the inner barrier, extending the lifetime of the WP to many thousands of years.

In support of the Nuclear Regulatory Commission High-Level Nuclear Waste Program, the Center for Nuclear Waste Regulatory Analyses is developing a performance assessment capability for the purpose of evaluating the overall performance of the proposed repository at YM. As part of the activities conducted initially in the Container Life and Source Term and later in the Total-System Performance Assessment and Integration Key Technical Issues, the Engineered Barrier System Performance Assessment Code (EBSPAC) Version 1.1 was developed as a deterministic code to provide a means for evaluating the WP lifetime and radionuclide release rates. A simple model, based on a parametric equation in which the parameter representing the efficiency of galvanic coupling controls the corrosion potential of the galvanic couple formed by the two metallic barriers, is used to evaluate the beneficial effect of galvanic coupling on WP life. The value of the efficiency parameter varies between 0.0 (no coupling) and 1.0 (perfect coupling). From the results of this simple model, galvanic coupling between the outer and inner metallic barriers was identified as a key factor in increasing the WP lifetime over a wide range of repository conditions.

An auxiliary analysis was performed in order to improve the mechanistic understanding of the effect of galvanic coupling, develop a methodology to estimate a reasonable range of values for the galvanic coupling efficiency, evaluate the adequacy of the DOE prediction of a substantive beneficial effect, and reduce the uncertainties involved in the EBSPAC calculations. The electrochemical kinetics of the anodic dissolution and cathodic reduction reactions were used to calculate both the corrosion potentials of the individual materials and the galvanic corrosion potentials of the materials when coupled. Corrosion potentials were calculated by summing all anodic and all cathodic reaction currents to zero because electrical charge cannot be accumulated in the metals. The anodic dissolution of A516 carbon steel was described by the active dissolution of iron whereas passive dissolution was assumed for alloy 825 (one of the primary candidates for the corrosion resistant barrier). The reduction reactions were considered limited to the reductions of water and oxygen. Evaluation of the effects of galvanic coupling was performed by considering the dissolution and reduction reactions occurring on both A516 carbon steel and alloy 825. The geometry of the galvanic couple was based on a through-wall pit penetrating the outer A516 carbon steel barrier that exposes the inner corrosion resistant alloy 825 to an acidified local environment. The gradient in chemical composition, and hence the variation of solution conductivity in the pit, was ignored to simplify the calculation. The criterion adopted for the occurrence of localized corrosion of the inner overpack material was conservatively based on the repassivation potential. If the galvanic corrosion potential of alloy 825 is lower than the repassivation potential, it is assumed that localized corrosion will not occur and the alloy will corrode slowly under passive dissolution conditions. A characterization of the galvanic couple in terms of the resistance between the WP

materials was developed by correlating the resistance of the galvanic couple with its efficiency. The resistance of the galvanic couple as a function of galvanic coupling efficiency was determined for all the parameters investigated and related to the resistivity of the pit solution. From the auxiliary analysis, it was concluded that to attain conditions where the localized corrosion of alloy 825 could be suppressed, resistance of the galvanic couple must be less than 500 ohms. For a material with a higher E_{rp} such as alloy 625, localized corrosion can be avoided by galvanic coupling even if the couple has a greater resistance and is, therefore, less efficient.

The objectives of the study reported here are to compare the results of modeling calculations to experimental tests in order to gain confidence in the calculated values, identify the need to refine the model calculations, and determine experimentally the effects of passive films, oxide scales, and corrosion products on the efficiency of the galvanic couple. Tests were performed with perfectly coupled galvanic specimens using a range of environmental parameters and material surface area ratios such that the results could be directly compared to the model calculations. Environmental parameters experimentally varied were temperature, pH, and partial pressure of oxygen. Reduction of the galvanic coupling efficiency as a result of oxide layers on the carbon steel and alloy 825 surfaces and corrosion products between the metal barriers was evaluated by measuring the corrosion potentials of each material during exposure in chloride containing solutions.

Results of the experimental investigations undertaken to examine the effects of environmental factors and area ratio were in agreement with the galvanic corrosion model predictions. Increasing the pH and partial pressure of oxygen resulted in higher corrosion potentials of the perfectly coupled specimens. Tests performed under deaerated conditions indicated significant reductions in the carbon steel corrosion rate and potential of the galvanic couple. Varying the temperature in the range of 25 to 95 °C did not significantly change either the carbon steel corrosion rate or the galvanic corrosion potential of the perfectly coupled specimens. Increasing the alloy 825/A516 steel area ratio by a factor of 10 increased the corrosion rate of the A516 steel barrier by a factor of 10 and increased the corrosion potential by 100 mV.

Corrosion potential tests conducted with polished A516 steel specimens in direct contact with polished and passivated alloy 825 specimens indicated that the solution pH in the range of 3 to 10.8 does not reduce the efficiency of the galvanic couple. However, the formation of a passive film on the A516 steel in alkaline solutions was observed to increase the corrosion potential of the galvanic couple by over 200 mV. Results from tests conducted with imperfectly coupled specimens showed conclusively that the presence of an oxide scale on the A516 steel and a passive film or thermal oxide on alloy 825 does not lower the efficiency of the galvanic couple. The galvanic coupling efficiency was reduced by the presence of a 1.5-mm thick layer of either corrosion products or iron oxides such as Fe_3O_4. Although significant reductions in the galvanic coupling efficiency were observed when a thick layer of corrosion products was placed between the materials, the corrosion potential of alloy 825 was continuously maintained below the repassivation potential for localized corrosion. These results indicate that the alloy 825 inner barrier will be protected from localized corrosion even with inefficient galvanic coupling to the carbon steel outer overpack.

1 INTRODUCTION

The waste packages (WPs) for disposal of high-level radioactive waste (HLW) at the proposed repository at Yucca Mountain (YM), Nevada, are expected to be designed to provide near complete containment for several thousand years after disposal. The WP consists of containers, fillers, basket materials, and waste forms [spent fuel (SF) or vitrified reprocessed waste]. The container lifetime is one of the important system attributes that needs to be assessed to determine overall repository performance.

Many factors, including WP design and interactions of the WP materials with the near-field repository environment, will have an effect on container lifetimes. The proposed HLW disposal containers consist of an inner overpack made of a corrosion-resistant material (CRM), with a 2.0-cm wall thickness, that will in turn be contained in an outer overpack made of a corrosion-allowance material (CAM) with a 10-cm wall thickness. Nickel-based alloys, such as alloys 825 (42Ni-22Cr-3Mo-29Fe), 625 (62Ni-22Cr-9Mo-5Fe), and C-22 (56Ni-22Cr-13Mo-3W-3Fe) are presently being evaluated for the inner corrosion-resistant overpack (Roy et al., 1996a). A carbon steel, A516 Grade 55, is proposed as the primary candidate material for the outer corrosion allowance overpack (TRW Environmental Safety Systems, Inc., 1996).

1.1 STUDIES CONDUCTED BY THE DEPARTMENT OF ENERGY

A literature review of galvanic corrosion has been published as part of the Degradation Mode Survey series for the HLW disposal containers (Roy et al., 1996b), in which data available in the open literature for some of the candidate materials are evaluated. In addition to a general discussion on some basic aspects of galvanic corrosion, information and data available on galvanic corrosion of carbon and low-alloy steels, Cu-Ni and Ni-Cu alloys, stainless steels (SS), Ni-based alloys, and Ti and its alloys are included. The results of all the studies reviewed can be summarized by stating that carbon or low-alloys steels would be anodic to any of the candidate inner overpack materials for all the range of plausible environmental conditions expected at the repository. This conclusion can be reached by noting that corrosion rate data in industrial, urban/rural, and marine atmospheres, as well as in natural and seawater at ambient temperatures, reveal that mild steel corrodes preferentially in these environments except when it is coupled to Mg or Zn. Data on corrosion of carbon steel in seawater at ambient temperature indicate that the corrosion rate increases significantly when it is coupled to alloys 400 (70Ni-30Cu), 600 (75Ni-16Cr-8Fe), and austenitic SS (types 304 and 316). From the results presented, Roy et al., (1996b) concluded that alloys 825 and 600 will be cathodically protected due to galvanic coupling to mild steel. They indicated that both alloys exhibit measurable corrosion rates in seawater, although no quantitative corrosion data were found for alloy 625. However, Scully and Hack (1984) have reported data for a galvanic couple made of steel and alloy 625 with an area ratio 1:1 and exposed to seawater at ambient temperature. A potential of –0.46 V_{SHE} was measured for the couple, which is an indication of preferential corrosion of the steel acting as an anode. It can be assumed that the same conclusion is applicable to alloy C-22.

Although a section on galvanic corrosion of welded joints is included in the review (Roy et al., 1996b), the information provided is insufficient to evaluate in detail the influence of welding on the galvanic corrosion of carbon steels. It is noted, however, that for carbon steels used in shipbuilding, the corrosion susceptibility in seawater of the heat-affected zone (HAZ) increases with increasing Mn content and decreasing welding temperature and heat input. The detrimental effect is the result of the decomposition of austenite at lower temperatures producing metastable microstructures containing bainite with retained

austenite or martensite. These low-temperature decomposition products will contain a greater amount of lattice defects than an equiaxed ferritic-pearlitic microstructure, making the HAZ more susceptible to corrosion. These observations supplemented with additional information should be considered in the evaluation of the fabrication and closure methods selected for the WPs.

Recently, the DOE has initiated an experimental program to evaluate galvanic corrosion arising from the interaction of dissimilar materials such as those proposed for the multibarrier WP design. Preliminary experiments currently are being performed using A516 steel as an anode and alloy 825 or G-3 (44N-22Cr-7Mo-1.5W-20Fe) as a cathode. Both metals forming the galvanic couple are connected by means of a potentiostat acting as a zero-resistance ammeter (ZRA) and exposed to an acidic brine at ambient temperatures (U.S. Department of Energy, 1997). No experimental results have been reported yet.

1.2 PREDICTION OF CONTAINER LIFETIMES

It is assumed in the DOE Total System Performance Assessment–1995 (TSPA-95), that exposure of the container to humid air or an aqueous environment results in uniform corrosion of the carbon steel overpack (TRW Environmental Safety Systems, Inc., 1995). Corrosion is assumed to proceed at a slow and predictable rate, and the occurrence of pitting corrosion is considered by using a pitting factor (TRW Environmental Safety Systems, Inc., 1995). Evaporation of the groundwater with presence of the heat generated by radioactive decay and interactions of the percolating water with concrete in the repository (not considered in TSPA-95), however, may result in an alkaline aqueous environment able to induce passivity of the carbon steel overpack. In the presence of chloride, passivity breakdown may occur leading to localized corrosion in the form of pitting (Marsh et al., 1986). Perforation of the carbon steel overpack will result in exposure of some areas of the CRM to an acidified aqueous environment enriched in chloride ions. Localized corrosion of the inner overpack can be mitigated by the use of both a highly corrosion-resistant alloy and its galvanic coupling to the carbon steel overpack (TRW Environmental Safety Systems, Inc., 1995; Mohanty et al., 1997).

Protection of the inner CRM by the remaining CAM used for the outer overpack has been recognized as one of the important design features of the WP. Cathodic protection has typically been used to protect steel structures such as gas pipelines, offshore oil platforms, and ship hulls as well as other types of components in many engineering applications (Morgan, 1993). As in any other cathodic protection application, the goal is to achieve the highest efficiency attainable in the galvanic coupling. Because the WPs are expected to perform for a period well beyond that acceptable for other engineering applications, a mechanistic understanding in conjunction with experimental testing will be useful in developing reasonable predictions. There are three general considerations in any cathodic protection scheme: (i) potential and current distribution or, indirectly, galvanic coupling efficiency and throwing power; (ii) anode life; and (iii) overprotection leading to hydrogen embrittlement.

Different approaches have been used by the DOE and the Center for Nuclear Waste Regulatory Analyses (CNWRA) to calculate the HLW container lifetimes. The DOE has performed a probabilistic analysis of container life in the TSPA-95 (TRW Environmental Safety Systems, Inc., 1995) using the Waste Package DEGradation (WAPDEG) Version 1.0 code (Atkins and Lee, 1996). WAPDEG is designed to run stochastic simulations, in which sampled parameter values are used to determine the WP failure time. A summary of the methodology used by the DOE to calculate the corrosion penetration of both the carbon steel outer overpack and the corrosion-resistant inner overpack has previously been reported (Dunn and Cragnolino, 1997). Humid air corrosion is considered to be corrosion that occurs under a thin water film

forming on the container surface above a critical relative humidity (RH) range uniformly distributed between 65 and 75 percent. Aqueous corrosion refers to corrosion of metal in contact with bulk water, assumed to occur at RHs greater than a threshold value uniformly distributed between 85 and 95 percent. The degree of cathodic protection of the inner overpack by the breached outer overpack is not determined by calculating the corrosion potential of the galvanic couple or potential and current density distributions as is commonly performed for cathodic protection of other engineered structures. Instead, it is assumed that once the outer container is breached by pits, cathodic protection of the inner overpack protects the CRM from pitting corrosion until the overall thickness of the outer metallic barrier is reduced by 75 percent. This criterion was adopted following an expert elicitation.

In the DOE calculations (TRW Environmental Safety Systems, Inc., 1995), performed with an aerial mass loading (AML) rate of 83 MTU/acre and an infiltration rate of 0.05 mm/yr, without backfill between the containers and the drift wall, the cumulative distribution function without galvanic protection exhibits the first WP failure at 2,200 yr and a median failure time of slightly over 3,000 yr with 92 percent of the WPs failing in 10,000 yr. If galvanic protection of the CRM by the outer CAM is considered, the first failure occurs after 8,000 yr, the median failure time is extended to 40,000 yr, and only 60 percent of the containers fail in 100,000 yr.

Calculations performed using CNWRA EBSPAC Version 1.1 (Mohanty et al., 1997) utilized kinetic expressions for the anodic and cathodic reactions occurring on the CRM. The corrosion potential of the CRM is the potential at which the magnitude of the total cathodic current is equal to the anodic dissolution current. Although the calculations were performed assuming the CRM to be alloy 825, the same methodology could be used for other CRMs provided the necessary electrochemical parameters are available. The effect of galvanic coupling on the performance of the WP is determined by calculating the galvanic corrosion potential of the bimetallic WP, E_{corr}^{WP}, as a function of the galvanic coupling efficiency, η, according to Eq. (1-1).

$$E_{corr}^{WP} = (1 - \eta)\, E_{corr}^{825} + \eta\, E_{couple} \qquad (1\text{-}1)$$

where

E_{corr}^{825} — Corrosion potential of the alloy 825 CRM barrier

E_{couple} — Galvanic corrosion potential of perfectly coupled alloy 825/A516 steel materials

The value of η can be 0 to 1 with higher numbers representing more efficient galvanic coupling. Based on the previous work of Scully and Hack (1984) who measured the galvanic corrosion potential of an alloy 625/carbon steel couple in seawater, the value of E_{couple} was assumed to be –0.462 V_{SHE}. Galvanic protection of the alloy 825 CRM barrier is achieved when the value of E_{corr}^{825} is less than the repassivation potential, E_{rp}, which has previously been demonstrated (Sridhar et al., 1995) to be the critical potential for the initiation of localized corrosion.

Calculations of container lifetimes by the CNWRA have been performed using a range of galvanic coupling efficiency coefficients, η, with an AML of 80 MTU/acre, no ventilation of the repository drifts or backfilling, and a critical RH of 65 percent for the onset of aqueous corrosion. For an η value of less than 0.2 (inefficient galvanic coupling), the calculated WP failure time is on the order of 2,700 yr. The WP life extends to over 10,000 yr if the value of η is greater than 0.2.

An auxiliary analysis (Dunn and Cragnolino, 1997) was performed in order to improve the determination of the galvanic corrosion potential, with specific emphasis placed on calculating the corrosion potential of a perfect galvanic couple of A516 steel and alloy 825 under a wide range of environmental conditions, instead of relying on literature data of Scully and Hack (1984) for this parameter. The dissolution rate and corrosion potential of the A516 steel outer overpack was also determined. Calculations were performed to predict the effect of environmental parameters such as temperature, pH, and oxygen concentration as well as the area ratios of the materials on the galvanic corrosion potentials as a function of the galvanic coupling efficiency. In addition, a method was developed to relate the efficiency of the galvanic couple to the resistance of the contact between the metals.

The objectives of this investigation were to verify the results obtained in the auxiliary analysis by performing galvanic corrosion tests with alloy 825 and A516 steel couples and to compare the measured galvanic corrosion potentials and corrosion rates to the calculated values. Baseline tests were conducted in order to measure the corrosion potential of a perfect galvanic couple under a range of environmental conditions. Corrosion potentials of the materials under imperfect coupling conditions were also measured in order to assess the reduction of galvanic coupling efficiency due to the presence of passive films, oxide scales, and corrosion products.

2 METHODS

2.1 GALVANIC CORROSION CALCULATIONS

Complete details of the modeling of galvanic coupling, selection of data, and the model calculations have been reported elsewhere (Dunn and Cragnolino, 1997). A summary is presented in the following sections.

Calculations of the corrosion potentials for the CRM and the CAM, as well as the galvanic corrosion potentials, were performed using the kinetics of the metal dissolution reaction and the cathodic reduction kinetics of both oxygen and hydrogen at the metal surface. Several simplifying assumptions were made in the calculation of the galvanic corrosion potentials:

- The galvanic couple is a one-dimensional system of two parallel plates consisting of a CRM (alloy 825) and a CAM (A516 steel).
- The current flow in the galvanic couple is perpendicular to the plates and hence the equipotential surfaces are parallel to the plates. This simplifying assumption was made in order to treat the problem analytically.
- The conductivity of the electrolyte is constant and does not contain any spatial variability related to concentration gradients.
- The corrosion of A516 steel is described by the active dissolution of iron.
- The dissolution of CRM occurs at a rate determined by the passive current density.
- Oxygen and water reduction are the only cathodic reactions. Oxygen reduction is controlled by a combination of surface activation and transport controlled reactions whereas water reduction is controlled only by surface activation.
- Pitting can penetrate 10-cm-thick carbon steel.

Groundwater contacting the containers may vary in pH as a result of many processes occurring in the repository near field. The interactions of the groundwater with concrete used in drift walls and inverts, as well as evaporative and refluxing effects associated with radioactive decay heat and rock fracture flow, may result in significant increases in pH (Mohanty et al., 1997). Alkaline aqueous solutions (pH $\geq$ 9) confer passivity to carbon steels, but the presence of chloride ions will result in localized corrosion of the A516 steel outer overpack above a critical potential, dependent on temperature and chloride concentration (Mohanty et al., 1997; Sridhar et al., 1994). Penetration of the carbon steel overpack by localized corrosion will result in the exposure of the CRM to an aqueous environment. The magnified schematic view of this through-wall pit penetrating the outer barrier is shown in figure 2-1. While the pit is active, dissolution of iron, shown in Eq. (2-1), occurs at the bottom of the pit. Hydrolysis of the Fe^{2+} species occurs inside the pits resulting in the formation of $FeOH^+$ and H^+. At the mouth of the pit, a membrane of Fe_3O_4 and FeOOH is formed that separates the bulk environment (i.e., near-field repository environment in contact with the containers) from the environment formed within the pit. This membrane is porous and allows the transport of soluble corrosion products out of the pit and the migration of Cl^- ions into the pit. The anion exchange

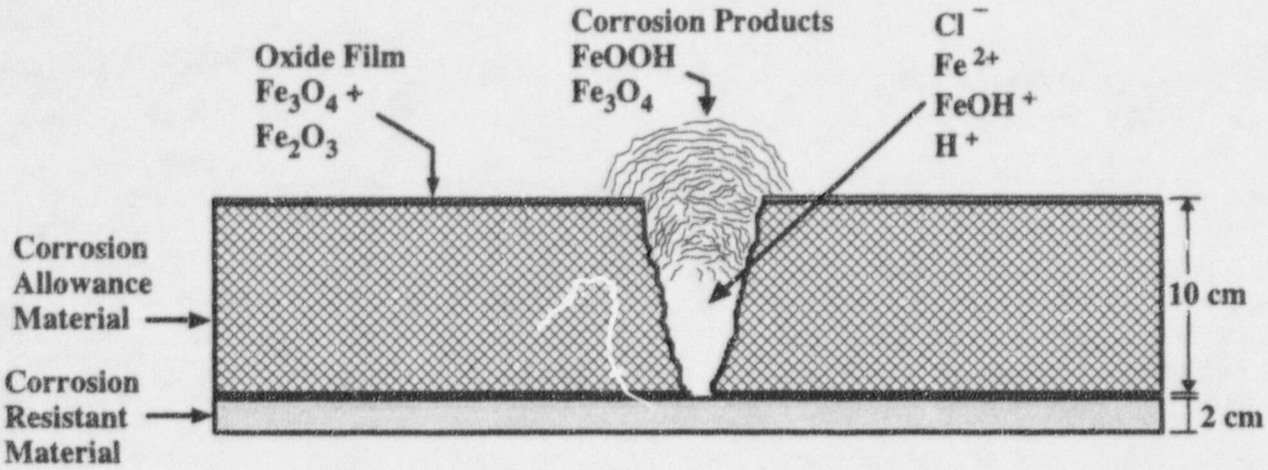

Figure 2-1. Schematic view of pit penetrating the outer A516 steel overpack with the mouth of the pit covered by corrosion products and a passive oxide film over the surface of the outer overpack

property of Fe_3O_4 has been discussed by Laycock et al., (1997). Outside the pit, the surface is passivated and covered with an oxide containing Fe_3O_4 and Fe_2O_3. The reduction of oxygen occurs on the outside surface near the mouth of the pit. This reaction is shown as Eq. (2-2).

$$Fe \rightarrow Fe^{2+} + 2e^- \tag{2-1}$$

$$O_2 + 2H_2O + 4e^- \rightarrow 4OH^- \tag{2-2}$$

Under acidic conditions, the reduction of hydrogen ions can occur as follows

$$2H^+ + 2e^- \rightarrow H_2 \tag{2-3}$$

After the pit penetrates the A516 steel, the area ratio of alloy 825 and A516 steel will depend on the relative areas of each material exposed to the electrolyte. For alloy 825, this area is defined by the radius of the electrolyte puddle contacting the CRM surface, r_{CRM}. The anodic area of A516 steel is determined by both the radius of the pit, r_p, and the height of the pit above the alloy 825 surface that is active, h_p. In these calculations, the r_p was assumed to be between 1 and 5 mm. The r_{CRM} varied between 5 and 50 mm. The h_p was assumed to be between 20 and 100 mm. With these limits, the area ratio of alloy 825 to A516 steel varies between 8:1 and 1:40.

The kinetics of both the metal dissolution along with the oxygen and water reduction reactions are used as the basis for calculating the galvanic corrosion potential of the multibarrier WP. The current density for the dissolution of the A516 steel CAM is described by the Tafel Equation (2-4):

$$i_{active}^{steel} = i_{0,Fe/Fe^{2+}} \left\{ \exp \left[\frac{\alpha_{Fe} z_{Fe} F \left(E - E_{Fe/Fe^{2+}} \right)}{RT} \right] \right\} \qquad (2\text{-}4)$$

where

$i_{0,Fe/Fe^{2+}}$ — exchange current density for the dissolution of iron
α_{Fe} — charge transfer coefficient for the dissolution of iron
z_{Fe} — number of electrons involved in the dissolution of iron
F — Faraday's constant
E — potential
$E_{Fe/Fe^{2+}}$ — equilibrium potential for the dissolution of iron
R — gas constant
T — temperature in K

The value of $i_{0,Fe/Fe^{2+}}$ has been reported by Heusler (1976) to be 10^{-10} A/m^2. Bockris et al., (1961) presented values in the range of 10^{-1} to 10^{-6} A/m^2, depending on the concentration of Fe^{2+}, pH, and the anionic species in solution. Conway (1952) noted values of 10^{-2} A/m^2 as being typical for the exchange current densities for the dissolution of iron and nickel. In the present model, a value of 10^{-4} A/m^2 was used for $i_{0,Fe/Fe^{2+}}$. The z_{Fe} is assumed to be 2 and α_{Fe} is assumed to be 0.5.

The cathodic current density for the reduction of oxygen on the metal surface, $i_{O_2}^{metal}$, is given by Eq. (2-5)

where

$$i_{O_2}^{metal} = i_{0,O_2}^{metal} \frac{\exp \left[\frac{-\beta_{O_2} z_{O_2} F \left(E - E_{O_2} \right)}{RT} \right]}{1 + \left\{ \frac{i_{0,O_2}^{metal} \delta \exp \left[\frac{-\beta_{O_2} z_{O_2} F \left(E - E_{O_2} \right)}{RT} \right]}{4 F D_{O_2} C_{O_2}^{bulk}} \right\}} \qquad (2\text{-}5)$$

i_{0,O_2}^{metal} — exchange current density for the reduction of oxygen
β_{O_2} — charge transfer coefficient for the reduction of oxygen
z_{O_2} — number of electrons involved in the reduction of oxygen
E_{O_2} — equilibrium potential for the reduction of oxygen

δ — thickness of the diffusion layer

D_{O_2} — diffusion coefficient for oxygen

$C_{O_2}^{bulk}$ — concentration of dissolved oxygen in the bulk solution

It is important to note that δ is not the water film thickness but rather the thickness of the diffusion layer across which a concentration gradient of oxygen exists. The value of δ for a stationary system is on the order of 5×10^{-4} m (Bockris and Reddy, 1977). This decreases with convection and for a well agitated system, δ can be as low as 5×10^{-5} m. The exchange current density for the reduction of oxygen on either A516 steel or alloy 825, i_{0,O_2}^{metal}, at any temperature, is calculated as follows

$$i_{0,O_2}^{metal} = i_{0,O_2(298)}^{metal} \exp\left[\frac{\Delta H_{a,O_2}}{0.001R}\left(\frac{1}{298} - \frac{1}{T}\right)\right] \qquad (2\text{-}6)$$

where

$i_{0,O_2,(298)}^{metal}$ — exchange current density for the reduction of oxygen on steel at 298 K

$\Delta H_{a,O_2}$ — activation enthalpy for the reduction of oxygen

From the work of Calvo and Schiffrin (1988), $i_{0,O_2,(298)}^{metal}$ measured on passivated iron is in the range of 1×10^{-6} A/m^2. Calvo (1979) reported the $\Delta H_{a,O_2}$ to be 40 kJ/mol.

The cathodic current density for the reduction of water on either A516 steel or alloy 825 is given by Eq. (2-7)

$$i_{H_2O}^{metal} = i_{0,H_2O} \exp\left[\frac{-\beta_{H_2O}\, z_{H_2O}\, F\left(E - E_{H_2O}\right)}{RT}\right] \qquad (2\text{-}7)$$

where

i_{0,H_2O} — exchange current density for the reduction of water

β_{H_2O} — charge transfer coefficient for the reduction of water

z_{H_2O} — number of electrons involved in the reduction of water

E_{H_2O} — equilibrium potential for the reduction of water

The exchange current density for water reduction at 298 K, $i_{0,H_2O(298)}$, is calculated as a function of pH according to Eq. (2-8).

$$i_{0,H_2O(298)} = 2\ F\ k_1\ [H^+]^{\beta_{H_2O}} \tag{2-8}$$

where k_1 has been reported by Bockris and Reddy (1977) to be 5.18×10^{-8} mol m^{-2} s^{-1} and $i_{0,H_2O(298)}$ is 10^{-2} A/m^2 at pH = 0. The exchange current density at any temperature can then be calculated according to Eq. (2-9).

$$i_{0,H_2O} = i_{0,H_2O(298)}\ \exp\left[\frac{\Delta H_{a,H_2O}}{0.001R}\left(\frac{1}{298} - \frac{1}{T}\right)\right] \tag{2-9}$$

where

$\Delta H_{a,H_2O}$ — activation enthalpy for the reduction of water

The value of $\Delta H_{a,H_2O}$ has been estimated by Macdonald and Urquidi-Macdonald (1990) to be 20 kJ/mol.

The corrosion potential of A516 carbon steel is calculated by combining Eqs. (2-4), (2-5), and (2-7) and solving for the potential, E, where the sum of the anodic dissolution current and the cathodic reduction currents equal zero. Similarly, the corrosion potential for alloy 825 is determined by combining the passive current density (assumed to be 10^{-3} A/m^2) for alloy 825 with Eqs. (2-5) and (2-7).

Calculation of the galvanic corrosion potentials was performed in a similar manner. The general equation for the potential of a perfect galvanic couple between A516 steel and alloy 825 is

$$\sum_{j=1}^{n} I_{a,j} - \sum_{j=1}^{n} I_{c,j} = \sum_{j=1}^{n} i_{a,j}^{a} A_{a,j} + \sum_{j=1}^{n} i_{a,j}^{c} A_{c,j} - \sum_{j=1}^{n} i_{c,j}^{a} A_{a,j} - \sum_{j=1}^{n} i_{c,j}^{c} A_{c,j} = 0 \tag{2-10}$$

where

$I_{a,j}$ — current from the jth anodic reaction

$I_{c,j}$ — current from the jth cathodic reaction

$i_{a,j}^{a}$ — current density of the jth anodic reaction at the anode

$i_{a,j}^{c}$ — current density of the jth anodic reaction at the cathode

$A_{a,j}$ — area of the anode for the jth reaction

$i_{c,j}^{a}$ — current density of the jth cathodic reaction at the anode

$i_{c,j}^{c}$ — current density of the jth cathodic reaction at the cathode

$A_{c,j}$ — area of the cathode for the jth reaction

In the present calculation, only the active area of the A516 steel is considered and the surface of alloy 825 is considered passive (Dunn and Cragnolino, 1997). The areas of the anode and cathode are considered to be independent of the reaction. The reduction of water and oxygen are assumed to occur on both the alloy 825 and the A516 steel surfaces. Under these assumptions, the expression in Eq. (2-10) reduces to

$$A^{\text{steel}}\, i_{\text{active}}^{\text{steel}} + A^{825}\, i_{\text{pass}}^{825} = \tag{2-11}$$

$$(A^{825}\, i_{H_2O}^{825} + A^{825}\, i_{O_2}^{825} + A^{\text{steel}}\, i_{H_2O}^{\text{steel}} + A^{\text{steel}}\, i_{O_2}^{\text{steel}})$$

where

A^{steel}	—	surface area of the A516 steel
A^{825}	—	surface area of alloy 825
i_{pass}^{825}	—	anodic current density for the passive dissolution of alloy 825
$i_{\text{active}}^{\text{steel}}$	—	anodic current density for the active dissolution of A516 steel
$i_{H_2O}^{\text{steel}}$	—	cathodic current density for the reduction of water on A516 steel
$i_{H_2O}^{825}$	—	cathodic current density for the reduction of water on alloy 825
$i_{O_2}^{\text{steel}}$	—	cathodic current density for the reduction of oxygen on A516 steel
$i_{O_2}^{825}$	—	cathodic current density for the reduction of oxygen on alloy 825

Thus, the potential of a perfect galvanic couple, E_{couple}, is the potential where the sum of the anodic and cathodic currents occurring on both alloy 825 and A516 steel is equal to zero. The formation of corrosion products, oxide scales, and the resistance of the electrolyte may result in an imperfect galvanic couple where a potential difference between the container materials exists. The relationship between the corrosion potential of the imperfectly coupled alloy 825 WP, $E_{\text{corr}}^{825,\text{WP}}$, and η has been assumed (Mohanty et al., 1997) to be:

$$E_{\text{corr}}^{825,\text{WP}} = (1 - \eta)\, E_{\text{corr}}^{825} + \eta\, E_{\text{couple}} \tag{2-12}$$

The value of η may vary from 0, corresponding to no galvanic coupling, to 1 for perfect galvanic coupling. Whatever the value of η, the sum of all anodic currents should be equal to that of the cathodic currents to maintain charge balance.

The resistance of the galvanic couple between the alloy 825 surface and the A516 steel material, R_{couple}, is calculated by dividing the potential difference between the materials by the absolute value of the cathodic current as follows:

$$R_{couple} = \left| \frac{E_{corr}^{825,WP} - E_{corr}^{steel,WP}}{\sum_{j=1}^{n} i_{c,j} A_{c,j}} \right| \qquad (2\text{-}13)$$

where

$E_{corr}^{steel,WP}$ — galvanic corrosion potential of the steel WP

Since the value of R_{couple} is not well known and it depends on the galvanic coupling conditions, experimental investigations were carried out to determine the value of this parameter.

2.2 EXPERIMENTAL INVESTIGATIONS

Galvanic corrosion tests were performed using alloy 825 and A516 steel specimens with the chemical compositions provided in table 2-1. Tests were conducted in 2L test cells with solutions containing either 0.028 (1,000 ppm) or 0.5 M NaCl under either air saturated or deaerated conditions. Solution pH was varied between 3 and 10.8 and temperature was either 25 or 95 °C. Prior to the start of the tests, a high-impedance electrometer was used to measure the corrosion potentials of the test specimens versus a saturated calomel electrode (SCE) that served as the reference electrode. The specimens were then galvanically coupled through a potentiostat functioning as a ZRA. After galvanically coupling the specimens, the potential of the galvanic couple and the galvanic corrosion current were recorded. Tests were conducted using alloy 825 to A516 steel area ratios in the range of 1:10 to 10:1. Each test was conducted for a period of 5 to 10 days. At the conclusion of the tests, the specimens were removed and visually inspected. The weight loss of each specimen was also measured.

The direct current (DC) resistance of various metallic contacts was measured to characterize imperfect coupling conditions. Identical specimens of either A516 grade 60 or alloy 825 were used in a two-electrode arrangement. Coupling conditions were examined including polished surfaces, thermally oxidized surfaces, and specimens covered with a mill scale. Additional tests were performed with a 1.5 mm O-ring placed between the specimens. The O-ring was used to contain either a Cl^- solution, corrosion products, or a combination of both solution and solid corrosion products.

Galvanic corrosion potential tests were also conducted using an alloy 825 to A516 steel area ratio of 1:1. The specimens were coupled under a variety of conditions ranging from intimately contacting polished surfaces to contacts containing mill scales, thermal oxides, and a variety of possible corrosion products contained in a 1.5-mm-thick O-ring placed between the specimens. The potential of each of the specimens in the couple was continuously recorded while immersed in air-saturated 1,000 ppm Cl^- solution.

Table 2-1. Composition of alloy 825 and A516 steel

Material	Fe	Cr	Ni	Mo	Cu	Mn	Ti	Si	S	C
Alloy 825	30.4	22.1	41.1	3.30	1.80	0.35	0.8	0.19	<0.001	0.01
A516 Steel	98.5	0.03	0.01	0.01	0.02	1.00	—	0.23	0.009	0.18

3 RESULTS

The results of calculations conducted to determine the effect of environmental variables on the calculated corrosion potentials of the container materials are shown in the form of Evans diagrams. The anodic dissolution and the cathodic reduction kinetics for both A516 steel and alloy 825 are shown on the same graph. Although the effects of the environmental parameters are shown on the same diagram, the anodic dissolution kinetics for each material are determined separately without galvanic interaction. The reduction kinetics of both O_2 and H_2O are assumed to have the same electrochemical parameters on both the A516 steel and alloy 825. Therefore, the kinetics of the reduction reactions plotted in the Evans diagrams are valid for either alloy 825 or A516 steel. The E_{corr} of the alloys is determined by the intersection of the anodic and cathodic curves (figure 3-1).

A second type of plot is used to present the results of the galvanic corrosion potential computations. In these representations, the $E_{corr}^{825,WP}$ and the $E_{corr}^{steel,WP}$ are plotted as functions of η. As previously indicated, when $\eta = 0$, $E_{corr}^{825,WP} = E_{corr}^{825}$ and $E_{corr}^{steel,WP} = E_{corr}^{steel}$. Likewise, when $\eta = 1$, $E_{corr}^{825,WP} = E_{corr}^{steel,WP}$. The localized corrosion repassivation potential (E_{rp}) for alloy 825 measured in a 1,000 ppm Cl^- solution at 95 °C is also included in the plots to indicate the values of η at which localized corrosion can be initiated (Dunn et al., 1997; Sridhar et al., 1995). As discussed previously by Mohanty et al., (1997), alloy 825 is susceptible to localized corrosion when $E_{corr}^{825,WP} > E_{rp}$ and the lifetime of the container is determined by the localized corrosion propagation rate. On the contrary, alloy 825 is considered to be immune to localized attack when $E_{corr}^{825,WP} < E_{rp}$ and the lifetime of the container is determined by the passive current density of the material. In addition to the galvanic corrosion potentials, the resistance of the galvanic couple, R_{couple}, is also shown in complementary plots as a function of η. It must be emphasized that the galvanic coupling efficiency relating the coupled potential to the open-circuit potential of alloy 825 and the corrosion potential of a perfect galvanic couple Eq. (2-12) is an assumed relationship. This assumption leads to a relationship between potentials of steel and alloy 825 to diverge linearly as η is decreased (figure 3-2a). The ohmic drop between the couple, dictated by the resistance, can be gauged by marking off the potential difference between the cathodic and anodic curve of A516 steel shown in figure 3-1 for increasing IR_{couple} drops (Dunn and Cragnolino, 1997). This difference in potential is highly nonlinear with respect to R because of the diffusion limited cathodic current. Hence, a nonlinear relationship between η and R_{couple} develops as shown in figure 3-2b.

The results of galvanic corrosion tests are shown as plots of E_{couple} and the galvanic corrosion current versus time. A comparison of the modeling calculations and the galvanic corrosion tests is also provided in table 3-1.

3.1 EFFECT OF TEMPERATURE

3.1.1 Model Calculations

Raising the temperature from 273 to 368 K (0 to 95 °C) increases the rates of both the iron dissolution and the O_2 and H_2O reduction reactions. The dissolved oxygen concentration is reduced and, hence, the electrode potential for the reduction of oxygen decreases. As shown in figure 3-1, a slight increase

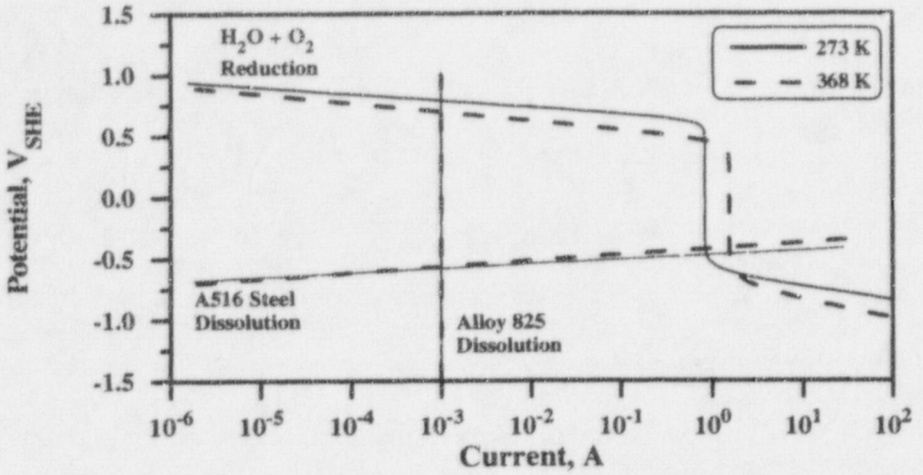

Figure 3-1. Evans diagram showing the effect of temperature in the range of 273 and 368 K (0 to 95 °C) on the calculated total cathodic current for the reduction of O_2 and H_2O, and anodic currents for the passive dissolution of alloy 825 and the active dissolution of A516 steel as a function of potential in an air-saturated solution of pH 5

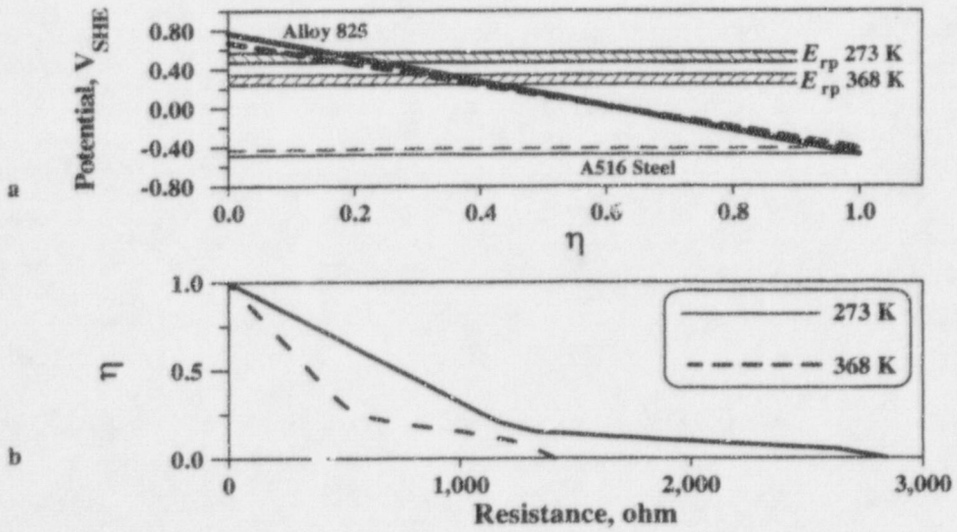

Figure 3-2. (a) Plot of the calculated galvanic corrosion potentials of alloy 825 and A516 steel as a function of the efficiency of the galvanic coupling, η, at two temperatures, 273 and 368 K (0 and 95 °C). Values of the repassivation potential, E_{rp}, of alloy 825 in 1,000 ppm chloride solutions are included. (b) Value of η as a function of the resistance of the galvanic couple showing the effect of temperature.

Table 3-1. Summary of calculated and measured galvanic corrosion potentials and corrosion current densities

Material	Area ratio 825:A516	Temp (°C)	pH	Air-saturated or deaerated solution	Cal. potential (mV vs SHE)	Cal. current density (A/cm^2)	Meas. potential (mV vs SHE)	Meas. current density (A/cm^2)	Meas. corr. rate (mm/year)
825/A516	1:1	95	5	air-saturated	-411	1.5×10^{-4}	-400 to -300	1.0×10^{-5} to 6.0×10^{-5}	0.12 to 0.69
825/A516	1:1	25	5	air-saturated	-460	8.5×10^{-5}	-350 to -280	6.0×10^{-5} to 1.0×10^{-4}	0.69 to 1.15
825/A516	1:1	95	5	deaerated	-490	3×10^{-6} to 5×10^{-6}	-480 to -420	3.0×10^{-6} to 2.0×10^{-5}	0.03 to 0.23
825/A516	10:1	95	5	air-saturated	-371	1.0×10^{-3}	-300 to -230	3.0×10^{-4} to 6.0×10^{-4}	3.45 to 6.9
825/A516	1:1	25	3	air-saturated	-450	1.6×10^{-4}	-360 to -310	1.0×10^{-5} to 5.0×10^{-5}	0.12 to 0.58
825/A516	1:1	95	3	air-saturated	-411	1.6×10^{-4}	-400 to -310	1.0×10^{-5} to 7.0×10^{-5}	0.12 to 0.80
A516 uncoupled		95	3	air-saturated	-422		-450 to -350		
825 uncoupled		95	3	air-saturated	+818		-100 to +300		

in the E_{corr}^{steel} is observed as the temperature rises due to both the change in the dissolution kinetics of iron and an increase in the diffusion-limited current for oxygen reduction. In contrast, the E_{corr}^{825} is inversely dependent on temperature as a result of the reduction in the dissolved oxygen concentration. These two opposite effects produce an increase of $E_{corr}^{steel,WP} = E_{corr}^{825,WP}$ of less than 100 mV when $\eta = 1$ (figure 3-2a). As shown in figure 3-2a, $E_{corr}^{825,WP}$ is a linear function of η as a result of the relationship assumed in Eq. (2-12). Also plotted in figure 3-2a is the E_{rp} of alloy 825 obtained in a 1,000 ppm chloride solution at 368 K. Under these conditions, E_{rp} is in the range of 0.24 to 0.34 V_{SHE} (Dunn et al., 1997). The active behavior of A516 steel is observed to dramatically reduce $E_{corr}^{825,WP}$ below E_{rp} for all values of $\eta > 0.3$. The most significant result occurring in the temperature range of interest, as illustrated in figure 3-2a, arises from the decrease in E_{rp}, from 0.50 ± 0.05 V_{SHE} to 0.29 ± 0.05 V_{SHE} as the temperature increases from 273 to 368 K (Dunn et al., 1997;

Sridhar et al., 1995). By comparing the plots of $E_{corr}^{825,WP}$ and the E_{rp} shown in figure 3-2a, it is evident that the propensity for localized corrosion of the alloy 825 waste container decreases by lowering the temperature, therefore requiring a far less efficient galvanic coupling to avoid the occurrence of localized corrosion.

In figure 3-2b, the value of η is plotted as a function of R_{couple}. It may be observed from this figure that, for low values of R_{couple}, η is close to 1.0 indicating a highly efficient galvanic couple. Figure 3-2b can be used to estimate the value of η provided that R_{couple} is known. For the two cases plotted in this figure, it is apparent that at higher temperatures, R_{couple} has to be lower to produce an efficient galvanic couple. This is primarily the result of the increased kinetics of both the O_2 and H_2O reduction reactions as the temperature is elevated. From figures 3-2a and 3-2b, it can be concluded that R_{couple} of 400 ohms will reduce η below 0.4 at a temperature of 368 K, and thus initiate localized corrosion of alloy 825.

3.1.2 Experimental Results

Galvanic corrosion tests performed in air-saturated, pH 5, 1,000 ppm Cl^- solutions at 25 and 95 °C using cylindrical alloy 825 and A516 steel specimens coupled through a ZRA are shown in figures 3-3a and 3-3b. Because there is no potential difference between the specimens, the galvanic coupling efficiency is 100 percent ($\eta = 1$). Since the A516 steel specimen is anodically polarized as a result of being coupled to alloy 825, and the passive current density for the alloy 825 specimen is approximately 2×10^{-7} A/cm^2, the galvanic current density plotted in figure 3-3a is essentially the corrosion current density for the A516 steel specimen. This is supported by post-test examination which revealed extensive corrosion of the A516 steel specimen and no indication of attack on the alloy 825 specimen. The E_{couple} shown in figure 3-3b is on the order of -0.360 V_{SHE} (-0.600 V_{SCE}). This compares well to the calculated galvanic corrosion potential of -0.400 V_{SHE} when $\eta = 1$ (figure 3-2a).

3.2 EFFECT OF SOLUTION pH

3.2.1 Model Calculations

After a pit has penetrated through the outer barrier, the pH of the solution contacting both alloy 825 and A516 is expected to be about 5 or lower due to the hydrolysis of Fe^{2+} cations. In figure 3-4, the effect of pH on E_{corr}^{825} and E_{corr}^{steel} is shown at pH values of 3 and 7. No significant change in E_{corr}^{steel} is observed. For simplicity, in the calculations provided in figure 3-4, it is assumed the dissolution of A516 steel is independent of pH within the 3 to 7 pH range. Figure 3-4, indicates that the main effect of decreasing the pH from 7 to 3 is an increase in E_{corr}^{825}. The effect of pH on the variation of $E_{corr}^{825,WP}$ and $E_{corr}^{steel,WP}$ with η is given in figure 3-5a. At low pH values, the E_{corr} of the WP materials is controlled by the reduction of H^+ ions. At near neutral pH, the reduction of O_2 is the most significant cathodic reduction reaction for both materials. At pH 3, localized corrosion of alloy 825 is possible for $\eta<0.5$, which in turn corresponds to a R_{couple} of 300 ohms (figure 3-5b). Localized corrosion of alloy 825 may only occur if $\eta<0.3$ at pH 7, which is the case of R_{couple} approximately equal to 450 ohms.

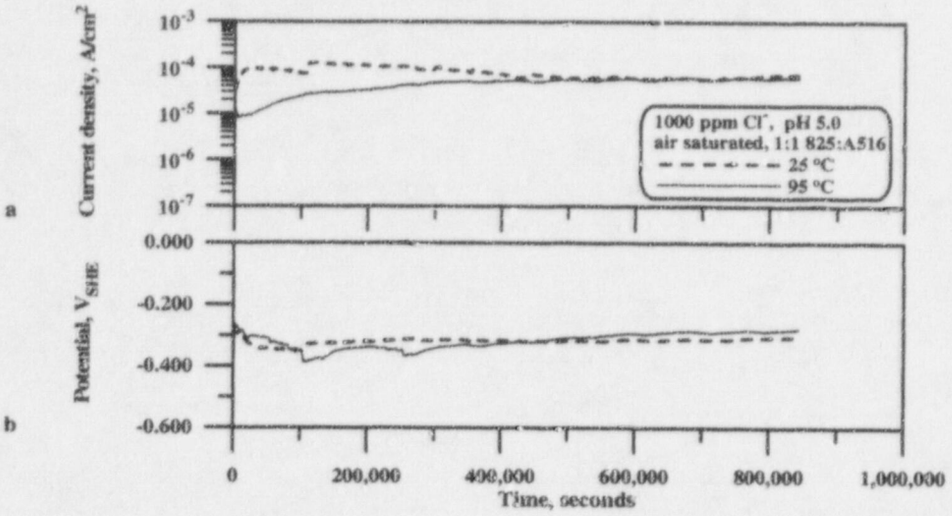

Figure 3-3. Galvanic corrosion tests conducted at 25 and 95 °C using alloy 825 and A516 steel specimens in air-saturated 1,000 ppm chloride solutions at pH 5. (a) Dissolution current density for A516 steel and (b) Galvanic corrosion potential.

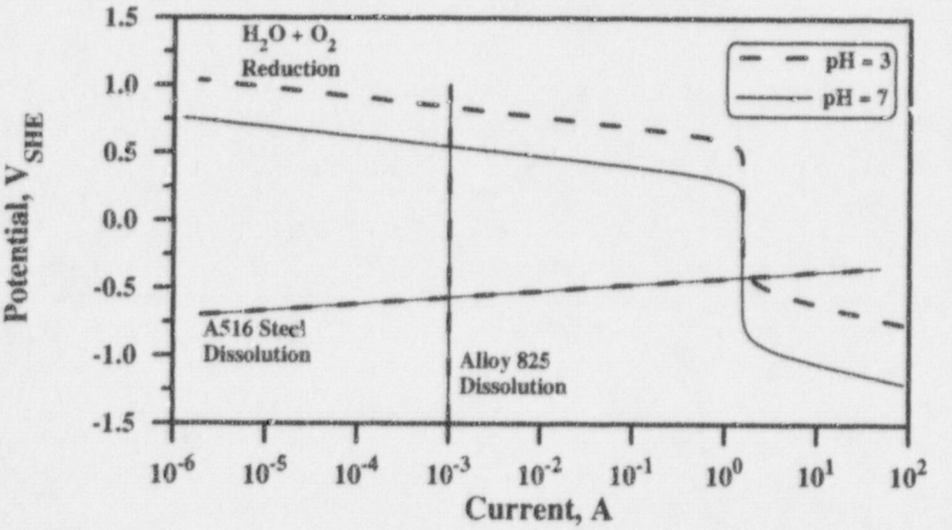

Figure 3-4. Evans diagram showing the effect of pH (3 and 7) on the calculated total cathodic current for the reduction of O_2 and H_2O, and anodic currents for the passive dissolution of alloy 825 and the active dissolution of A516 steel as a function of potential in an air-saturated solution at 368 K (95 °C).

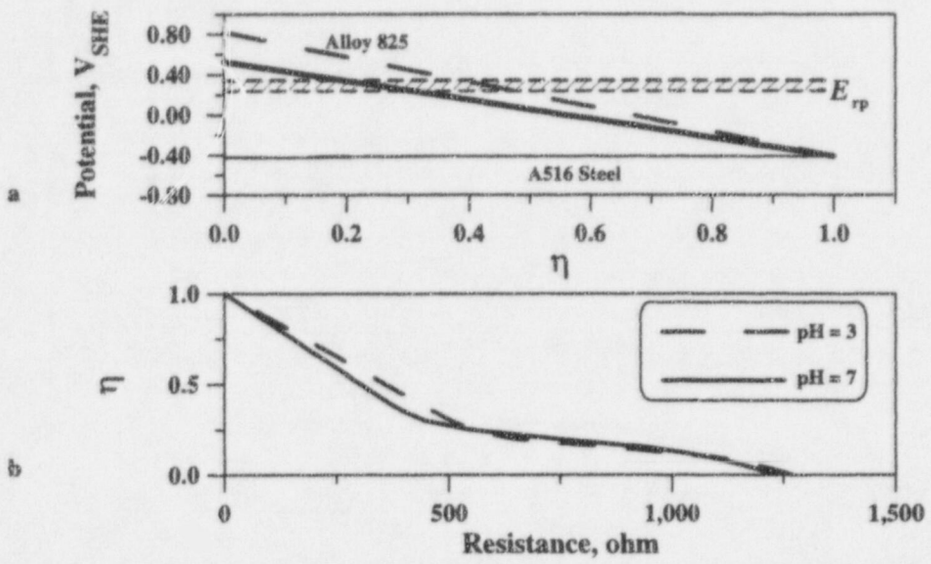

Figure 3-5. (a) Plot of the calculated galvanic corrosion potentials of alloy 825 and A516 steel as a function of the efficiency of the galvanic coupling, η, at two pH values (3 and 7). Values of the repassivation potential, E_{rp}, of Alloy 825 in 1,000 ppm chloride solutions at 368 K (95 °C) are included. (b) Value of η as a function of the resistance of the galvanic couple for two pH values (3 and 7).

3.2.2 Experimental Results

The results of the galvanic corrosion tests where $\eta = 1$ using solution pH values of 3.0 and 10.9 are shown in figures 3-6a and 3-6b. The potential and galvanic current density recorded in the test conducted at pH 3 is quite similar to those for the test conducted at pH 5 shown in figures 3-3a and 3-3b. It should be noted that the galvanic corrosion potential calculations indicate that the value of E_{couple} ($\eta = 1$) is constant over the pH range from 3 to 7 and has a predicted value of -0.400 V_{SHE} (-0.640 V_{SCE}) as indicated in figure 3-5a. At pH values above 9, the kinetics of steel dissolution are altered due to the formation of a stable passive film. These conditions were investigated by measuring the galvanic corrosion current and potential in a 1,000 ppm Cl^- solution at pH 10.9. The passivity of A516 steel is evident by the decrease in the corrosion current density to 10^{-6} A/cm^2 (figure 3-6a). The value of E_{couple} also increased to values in the range of -0.200 to -0.070 V_{SHE} (-0.440 to -0.310 V_{SCE}). At the conclusion of the test, areas of localized corrosion were observed on the A516 steel specimen while the alloy 825 specimen was not attacked.

3.3 EFFECT OF PARTIAL PRESSURE OF OXYGEN

3.3.1 Model Calculations

The effect of p_{O_2} on the E_{corr} of both materials is shown in figure 3-7. The E_{corr}^{825} is much higher than E_{corr}^{steel} when the solution is in equilibrium with air (p_{O_2} = 0.21 atm). When the p_{O_2} is reduced to 2.1×10^{-5} atm, which represents a well deaerated condition, the primary reduction reaction is switched from

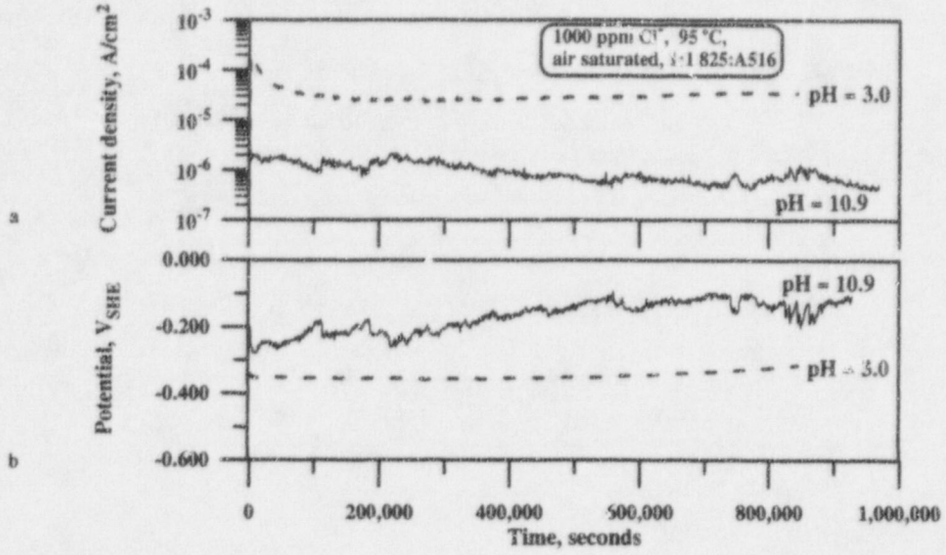

Figure 3-6. Galvanic corrosion tests conducted in air-saturated 1,000 ppm chloride solutions at pH 3 and 10.9 using alloy 825 and A516 steel specimens. (a) Dissolution current density for A516 steel and (b) Galvanic corrosion potential

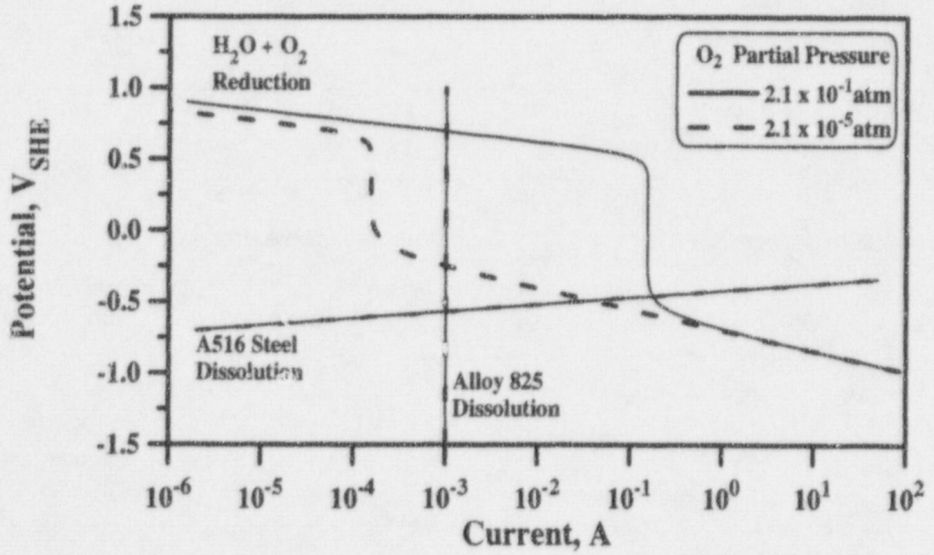

Figure 3-7. Evans diagram showing the effect of partial pressures of oxygen (2.1×10^{-1} and 2.1×10^{-5} atm) on the calculated total cathodic current for the reduction of O_2 and H_2O, and anodic currents for the passive dissolution of alloy 825 and the active dissolution of A516 steel as a function of potential in a solution of pH 5 at 368 K (95 °C).

the reduction of O_2 to the reduction of H_2O. Deaeration reduces the E_{corr}^{825} by almost 1.0 V and also reduces both the E_{corr}^{steel} and the I_{corr}^{steel}. In the case of a completely deaerated environment ($p_{O_2} \rightarrow 0$ atm), the E_{corr} of both WP materials is only determined by the kinetics of the metal dissolution and H_2O reduction reaction. Figure 3-8a presents the effect of the p_{O_2} on the galvanic corrosion potentials of the WP materials. Decreasing the p_{O_2} reduces the diffusion-limited current for the reduction of O_2, resulting in a lowering of the galvanic corrosion potentials. As indicated in figure 3-8a, when the p_{O_2} is less than 2.72×10^{-4} atm, the $E_{corr}^{825,WP}$ is always lower than the E_{rp}. In figure 3-8b, η is plotted as a function of R_{couple} for the air-saturated and partially deaerated cases provided in figure 3-8a. For the deaerated case in figure 3-8b, it is seen that the value of η remains close to 1 unless the R_{couple} is greater than 5,000 ohms. This result indicates that the value of η under deaerated conditions is consistently high and galvanic protection of the inner overpack can be assured.

3.3.2 Experimental Results

Tests conducted under both air-saturated and deaerated conditions are shown in figures 3-9a and 3-9b. As expected, the galvanic corrosion current decreased by over an order of magnitude when the solution was deaerated. In addition, the E_{couple} decreased to $-0.430\ V_{SHE}$ under deaerated conditions. Clearly the results of the galvanic corrosion tests are in agreement with the calculated values of the galvanic corrosion potential.

3.4 EFFECT OF AREA RATIO

3.4.1 Model Calculations

Figure 3-10a provides results of galvanic corrosion calculations for two surface area ratios of alloy 825 and A516 steel corresponding to the extremes expected for the geometry of the galvanic couple. The active behavior of the A516 steel reduces $E_{corr}^{825,WP}$ below E_{rp} for all values of $\eta > 0.35$. The effect of the area ratio is minimal, however, resulting at the most in a 100 mV increase in both $E_{corr}^{825,WP}$ and $E_{corr}^{steel,WP}$ with a 500 times decrease in the area ratio when $\eta \rightarrow 1$, but no change for $\eta \rightarrow 0$. It is apparent from this figure that the value above which localized corrosion is avoided ($\eta \approx 0.35$) is not strongly affected by the change in the area ratio.

The values of η determined from R_{couple} for the extremes of the area ratios considered in this study are graphically depicted in figure 3-10b. For an alloy 825:A516 steel area ratio of 12.5:1, a linear relationship between η and R_{couple} is observed. In this case, the value of R_{couple} necessary to initiate localized corrosion of alloy 825 is approximately 300 ohms. When the area of A516 steel is many times greater than that of alloy 825, however, localized corrosion can be initiated with a lower value of R_{couple}, on the order of 150 ohms.

3.4.2 Experimental Results

Galvanic corrosion tests conducted using two area ratios are shown in figures 3-11a and 3-11b. Increasing the alloy 825:A516 steel area ratio from 1:1 to 10:1 resulted in an order of magnitude increase in the corrosion rate of A516 steel. The value of E_{couple}, however, increased by less than 100 mV from $-0.360\ V_{SHE}$ to $-0.270\ V_{SHE}$, confirming the results of the calculations for $\eta = 1$ shown in figure 3-10a.

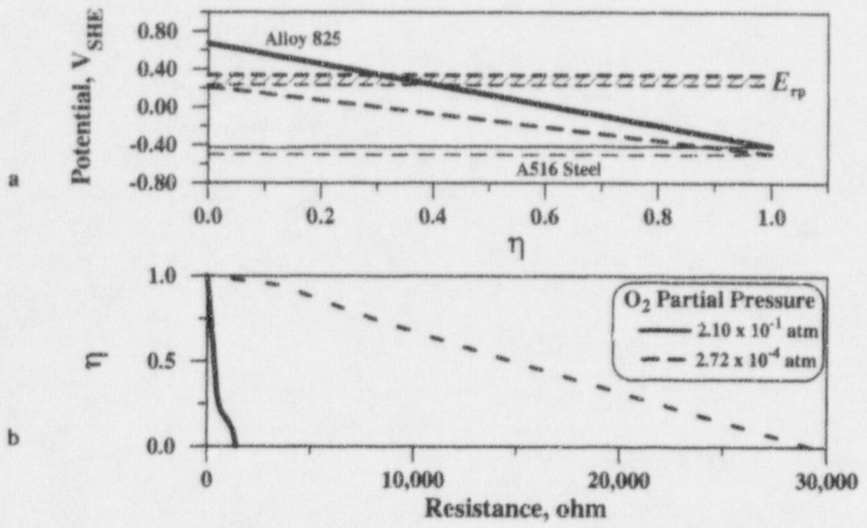

Figure 3-8. (a) Plot of the calculated galvanic corrosion potentials of alloy 825 and A516 steel as a function of the efficiency of the galvanic coupling, η, at two partial pressures of oxygen (2.1×10^{-1} and 2.72×10^{-4} atm). Values of the repassivation potential, E_{rp}, of alloy 825 in 1,000 ppm chloride solutions at 368 K (95 °C) are included. (b) Value of η as a function of the resistance of the galvanic couple for partial pressures of oxygen.

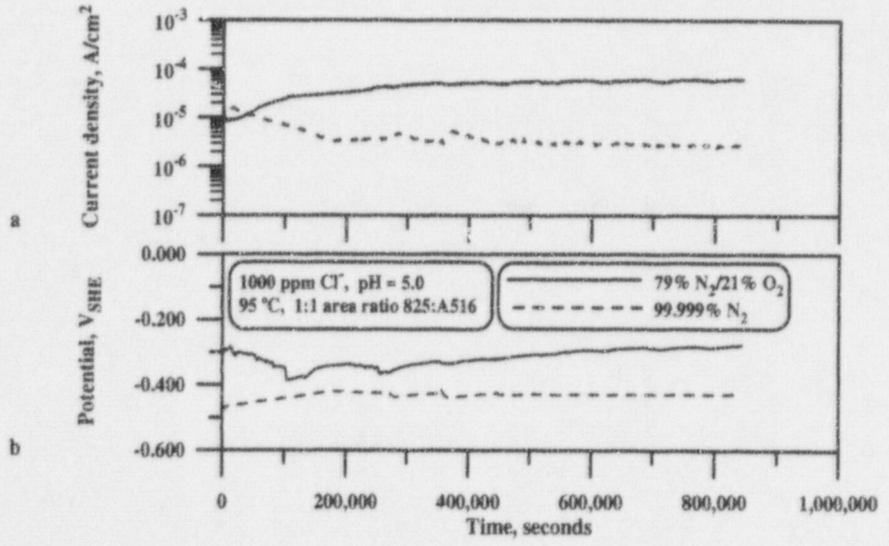

Figure 3-9. Galvanic corrosion tests conducted in 1,000 ppm chloride solutions at pH 5 under air-saturated and deaerated conditions using alloy 825 and A516 steel specimens. (a) Dissolution current density for A516 steel and (b) Galvanic corrosion potential.

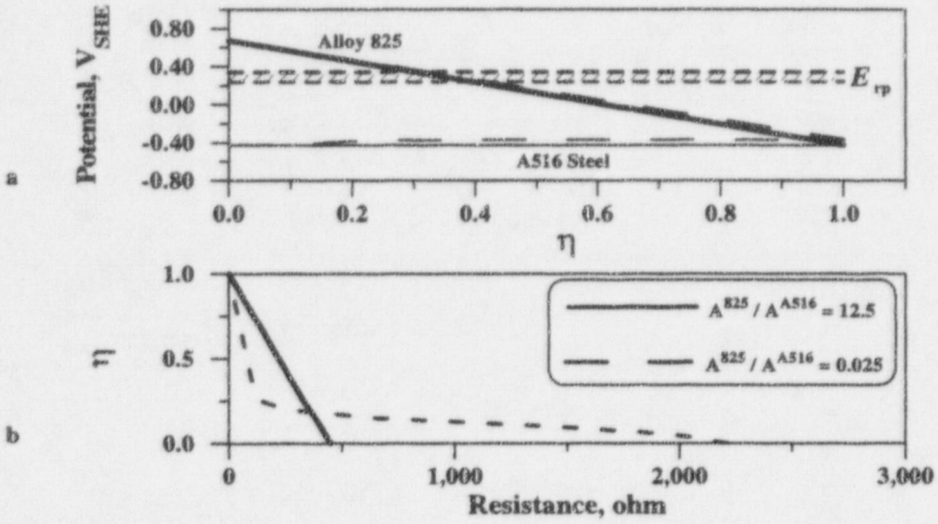

Figure 3-10. (a) Plot of the calculated galvanic corrosion potentials of alloy 825 and A516 steel as a function of the efficiency of the galvanic coupling, η, at two values of the surface area ratio between alloy 825 and A516 steel (12.5 and 0.025). Values of the repassivation potential, E_{rp}, of alloy 825 in 1,000 ppm chloride solutions at 368 K (95 °C) are included. (b) Value of η as a function of the resistance of the galvanic couple for two alloy 825/A516 steel surface area ratios.

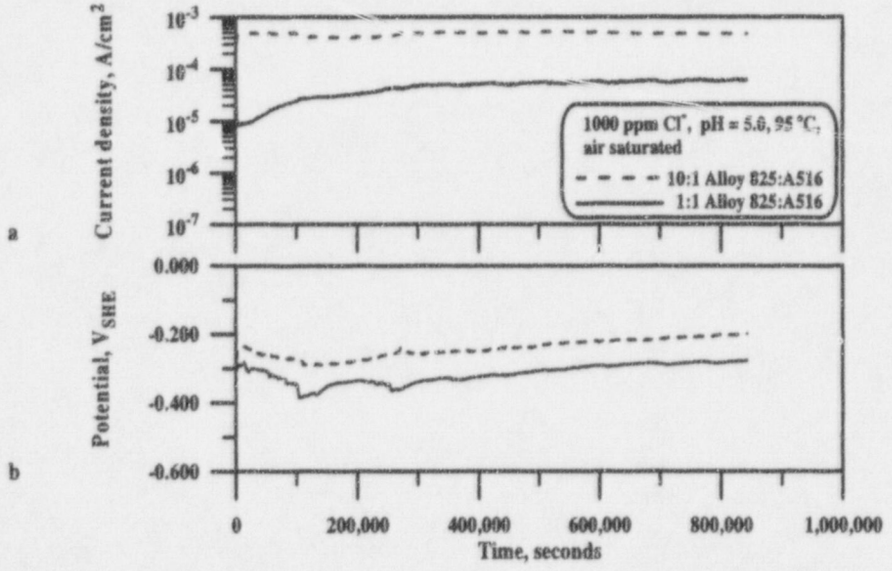

Figure 3-11 . Galvanic corrosion tests conducted in air-saturated 1,000 ppm chloride solutions with two area ratios using alloy 825 and A516 steel specimens. (a) Dissolution current density for A516 steel and (b) Galvanic corrosion potential.

3.5 RESISTANCE OF THE GALVANIC COUPLE

3.5.1 Model Results

The results of both the galvanic corrosion tests and model calculations suggest that as long as a highly efficient galvanic couple of A516 steel and alloy 825 is maintained, the potential of alloy 825 will be continuously held below the repassivation potential. There are, however, two possible limitations to the galvanic protection of the inner corrosion-resistant barrier by the CAM. First, complete consumption of the outer CAM will end galvanic protection. The time required for complete consumption is dependent on the corrosion rate of the outer barrier, which is, in turn, dependent of the exposure environment and the efficiency of the galvanic coupling. With efficient galvanic coupling, the potential of the A516 steel barrier is shifted to higher potentials. As a result, the corrosion rate of A516 also increases according to Eq. (2-3). The second limitation is the efficiency on the galvanic coupling. With the exception of the case in which the environment has a $p_{O_2} < 2.7 \times 10^{-4}$ atm, galvanic corrosion potential calculations suggest that an inefficient galvanic couple ($\eta < 0.4$) will result in the possible localized corrosion of the inner CRM barrier (i.e., $E_{corr}^{825,WP} > E_{rp}$). Poor galvanic efficiency may be caused by a highly resistive contact between the container materials. R_{couple} defined in Eq. (2-13) (Dunn and Cragnolino, 1997), is the sum of all the resistances between the WP barriers, as given by Eq. (3-1)

$$R_{couple} = R_{soln} + R_{CAM\ oxide} + R_{CRM\ oxide} + R_{corr\ product} \tag{3-1}$$

where

R_{soln} — resistance of the solution
$R_{CAM\ oxide}$ — resistance of the oxide on the CAM barrier
$R_{CRM\ oxide}$ — resistance of the oxide on the CRM barrier
$R_{corr\ product}$ — resistance of the corrosion products between the WP barriers

The resistance of the oxides and corrosion products may have a capacitive component instead of being purely resistive as in the case of the electrolyte. The solution resistance can be determined from the

$$R_{soln} = \rho_{soln} \frac{l}{A} \tag{3-2}$$

resistivity of the electrolyte (the inverse of the ionic conductivity) and the geometry of the galvanic couple according to the following equation:
where

ρ_{soln} — resistivity of the solution in ohm m
l — length between the anode materials constituting the galvanic couple
A — area

If only the electrolyte resistivity is considered in Eq. (3-1), $R_{couple} = R_{soln}$. According to the geometrical dimensions, l can vary from a low value to 0.1 m (i.e., the thickness of the A516 steel barrier). The value of A corresponds to the area of alloy 825 exposed to the pit environment. A value of 7.8×10^{-5} m^2, obtained when r_{CRM} = 5 mm, was used in this calculation. The value of ρ_{soln} may range from 5×10^{-5} to 1×10^{-2} ohm m, taking into consideration that the resistivity of a 5 mol/L $FeCl_2$ solution (the solution composition within a pit in steel) is 5×10^{-5} ohm m. For this specific geometry, the value of R_{soln} ranges from a very low value to approximately 13 ohms. The low resistance provided by the solution suggests that galvanic protection will be maintained under these conditions. Obviously, the major impediments to the flow of current result from the other resistance terms in Eq. (3-1).

3.5.2 Resistance Measurements

Resistance measurements were used to characterize imperfect galvanic coupling. Two specimens of the same material (either alloy 825 or A516 steel) were placed directly against each other. Tests were also performed with an O-ring, placed between the specimens, that was used to contain chloride solutions, corrosion products, or both the solutions and corrosion products. The resistance measured for the various specimen contact conditions is given in table 3-2. From the data shown in table 3-2, it is evident that the resistance of a polished metal surface is quite low. After thermal oxidation at 250 °C, however, the resistance of the A516 steel contact increased significantly. A much higher resistance (17.2 k ohms) was observed when specimens coated with a mill scale contacted together. The mill scale is likely to be porous, however, and when a 1,000 ppm Cl^- solution, contained in a 1.5-mm-thick O-ring, is placed between the A516 steel surfaces, the resistance drops to 0.75 k ohm. If dry corrosion products, generated by immersing an A516 steel specimen in a 1,000 ppm Cl^- solution, were placed in the O-ring, the resistance was 88.7 k ohm. The resistance decreased to 1.4 k ohm when a 1,000 ppm Cl^- solution was added to the A516 steel corrosion products. When dry $FeCl_2 \cdot 4H_2O$ was placed between the specimens the resistance was 2.4 k ohms. Adding a 1,000 ppm chloride solution to the $FeCl_2 \cdot 4H_2O$, which can be expected to produce a near saturated solution of $FeCl_2$, resulted in a resistance of 70 ohms. The resistances of a 1.5-mm-thick layer of powdered Fe_3O_4 and γ-FeOOH were extremely high. When a 1,000 ppm chloride solution was added, however, the resistances of the contacts were substantially reduced.

The results of galvanic corrosion potential tests conducted with polished A516 steel specimens in intimate contact with alloy 825 are shown in figure 3-12. For all of the tests shown, the potential of both materials were identical. The potentials were observed to increase with pH. In the aerated 1,000 ppm Cl^- solution at pH 3, the potential of the galvanic couple was in the range of −0.360 to −0.400 V_{SHE} (−0.600 to −0.640 V_{SCE}). In a pH 8 solution, the galvanic corrosion potential was in the range of −0.360 to −0.260 V_{SHE} (−0.600 to −0.500 V_{SCE}). The increase in the galvanic corrosion potential can be attributed to a change in the dissolution kinetics of the A516 steel. Active dissolution with a Tafel slope of 40 mV/decade of current occurs in solutions where the pH < 8. Above pH 8, carbon steel can become passive resulting in larger slopes in the polarization curves and higher corrosion potentials. The intimate contact between the specimens assures that the galvanic corrosion potential will be determined by the corrosion potential of the more active material. For the test conducted at pH 8, the pH of the solution actually increased to a value of 9.1 at the end of the test. This results in an increase in the galvanic corrosion potential throughout most of the test duration. A sharp decrease in the galvanic corrosion potential, observed at the end of the test, can be attributed to the breakdown of the passive film on the A516 steel specimen leading to active dissolution. Throughout most of the tests conducted at pH 10.8, the galvanic corrosion potential oscillated from −0.310 to −0.160 V_{SHE}. The large decreases in the galvanic corrosion potential can again be attributed to the breakdown of the

Table 3-2. Resistance of various metal contacts

Material	Contact Conditions	Exposed Area (cm^2)	DC Resistance (k ohms)
Alloy 825	Polished metal	7.9	<0.01
Alloy 825	100 °C thermal oxide, 7 days	7.9	<0.01
Alloy 825	250 °C thermal oxide, 7 days	7.9	<0.01
A516 Steel	Polished metal	7.9	<0.01
A516 Steel	100 °C thermal oxide, 7 days	7.9	<0.01
A516 Steel	250 °C thermal oxide, 7 days	7.9	0.11
A516 Steel	Mill scale	7.9	17.2
A516 Steel	Mill scale w/O-ring containing 1,000 ppm Cl^-	2.3	0.75
A516 Steel	Polished w/O-ring containing dry corrosion products[a]	2.3	88.7
A516 Steel	Polished w/O-ring containing corrosion products[a] + 1,000 ppm Cl^- solution	2.3	1.38
A516 Steel	Polished w/O-ring containing dry $FeCl_2 \cdot 4H_2O$ powder	2.3	2.41
A516 Steel	Polished w/O-ring containing $FeCl_2 \cdot 4H_2O$ + 1,000 ppm Cl^- solution	2.3	0.07

[a]Corrosion products from A516 steel in 1,000 ppm Cl^- solution.

passive film on A516 steel at high potentials. At low potentials, the passive film reforms on the A516. The formation of a stable passive film decreases the rate of the iron dissolution reaction, increases the slope of the potential versus current curves, and results in a higher corrosion potential.

Galvanic corrosion potential tests conducted with thermally oxidized alloy 825 specimens and A516 steel specimens covered with a mill scale are shown in figure 3-13. At pH 3, there is initially a potential difference of 170 mV between the alloy 825 and A516 steel specimens. The potential of A516 steel varied in the range of −0.410 to −0.360 V_{SHE} throughout the test. After approximately 1 day, the potential difference between the specimens was on the order of 20 mV. At pH 10.8, the initial potential difference between the specimens was 50 mV. The galvanic corrosion potential increased by over 100 mV during the test. Variations in the galvanic corrosion potential were also large and comparable to that of the polished surfaces shown in figure 3-12. The large potential variations can again be attributed to the breakdown and repassivation of the passive film on the A516 steel specimen. Similar results were obtained using polished and HNO_3 passivated alloy 825 and A516 steel specimens covered with a mill scale.

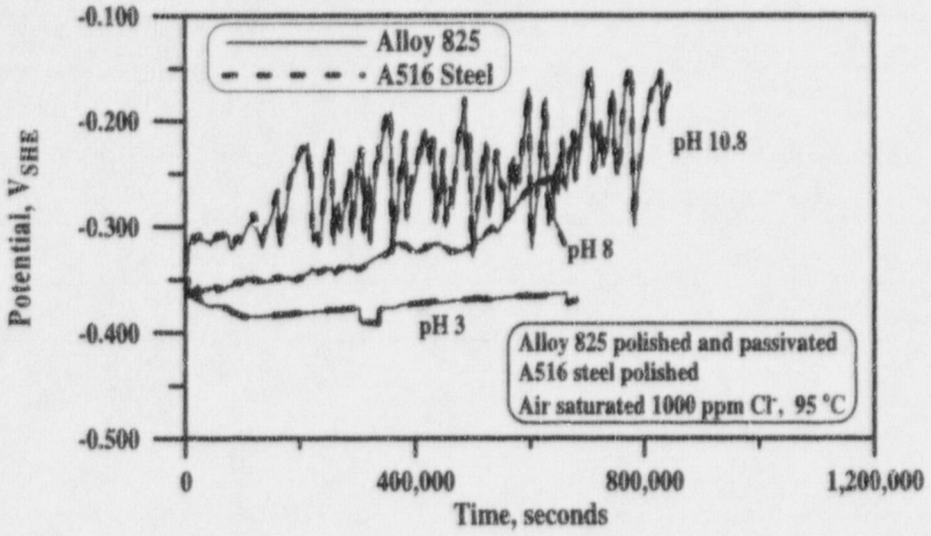

Figure 3-12. Corrosion potential of galvanically coupled alloy 825/A516 steel specimens in air- saturated 1,000 ppm Cl^- solutions at various pH values. Test specimens were in direct contact with each other.

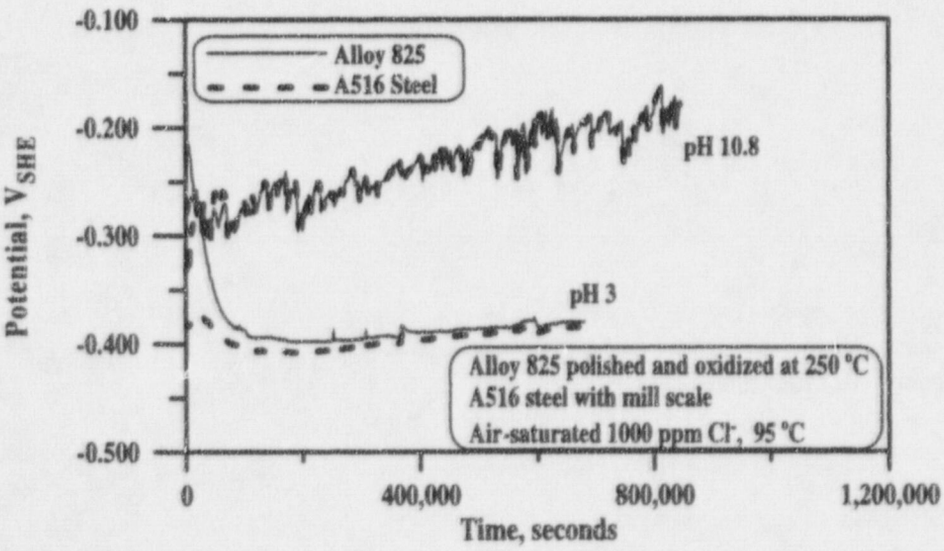

Figure 3-13. Corrosion potentials of galvanically coupled alloy 825/A516 steel specimens in air-saturated 1,000 ppm Cl^- solutions at 95 °C. Test specimens were connected through mill scale on A516 steel surface and thermal oxide on alloy 825 surface.

Figure 3-14 shows the results of open-circuit tests conducted with uncoupled specimens in an air-saturated 1,000 ppm Cl^- solution adjusted to pH 3. The alloy 825 specimen was polished to a 600 grit finish and passivated in HNO_3. The A516 steel specimen was tested with a mill scale present on two surfaces. Previous calculations indicated that the open-circuit potentials of both alloy 825 and A516 steel increase as the solution becomes more acidic. In addition, larger differences in the open-circuit potentials of the two materials are expected as solution pH decreases. From the open-circuit potential measurements shown in figure 3-14, it is apparent that the corrosion potential of alloy 825 is in the range of 0.200 to 0.300 V_{SHE} whereas the open-circuit potential of A516 steel is −0.400 to −0.360 V_{SHE}. Since the specimens are not coupled, the corrosion potential of alloy 825 is not reduced through galvanic interactions with A516 steel. During the majority of the test, the corrosion potential of the alloy 825 specimen was 0.6 to 0.7 V higher than the corrosion potential for A516 steel. The high corrosion potential of alloy 825 may also lead to localized corrosion during prolonged exposure times.

Also shown in figure 3-14 is a test conducted using polished and passivated alloy 825 and an A516 steel specimen with a mill scale. The surface of the alloy 825 specimen was placed in contact with the mill scale covered surface of the A516 steel specimen. Initially, the potential of the alloy 825 specimen was 0.2 V greater than the A516 steel specimen. After approximately 1 day, the potential of the two specimens are in the range of −0.400 to −0.360 V_{SHE}, indicating a highly efficient galvanic coupling.

Figure 3-15 shows the results of tests conducted with 1.5-mm-thick O-rings placed between the alloy 825 and A516 steel specimens. The O-ring, with an inside area of 2.3 cm^2, was filled with either corrosion products generated during the exposure of A516 steel to a 1,000 ppm Cl^- solution or reagent grade iron oxides and hydroxides. Prior to assembling the galvanic couple, 0.2 mL of a 1,000 ppm Cl^- solution was also placed within the O-ring. Alloy 825 specimens were polished to a 600 grit finish and passivated in HNO_3, whereas the A516 steel specimens were covered with a mill scale. With A516 corrosion products placed in the O-ring, large differences in the corrosion potentials of the specimens were observed. Initially the potential of the alloy 825 specimen was −0.010 V_{SHE} while the potential of the A516 steel specimen was −0.380 V_{SHE}. After approximately 2 days, the potential of alloy 825 rose to −0.230 V_{SHE}. After 700,000 s, the potential of alloy 825 slowly decreased. At the conclusion of the 2-wk test the potential of the alloy 825 specimen was −0.050 V_{SHE}, approximately 0.340 V higher than the A516 steel specimen. When the O-ring was filled with an iron oxide such as Fe_3O_4 and Fe_2O_3 (with the addition of 1,000 ppm Cl^- solution) large differences in the corrosion potentials of the specimens again were observed. The corrosion potential of alloy 825 was above 0.000 V_{SHE} when coupled to A516 steel through a 1.5-mm-thick layer of Fe_3O_4 in an air-saturated 1,000 ppm Cl^- solution indicating inefficient galvanic coupling.

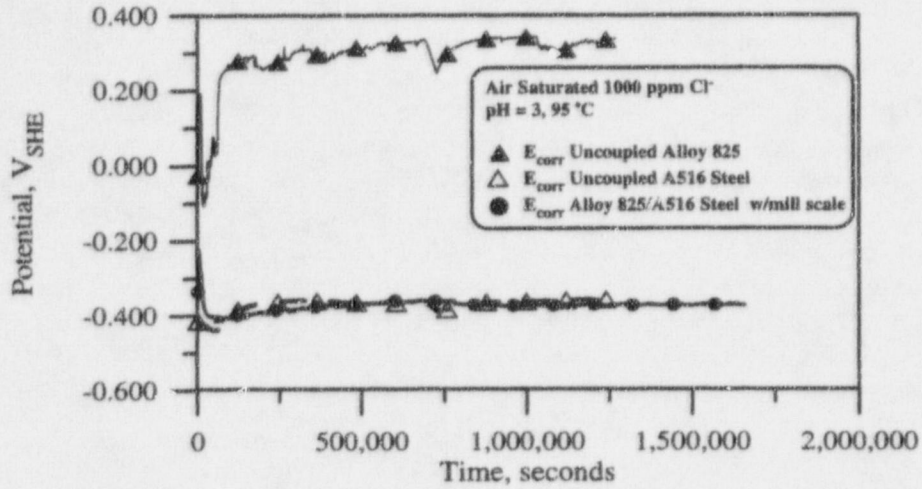

Figure 3-14. Comparison of corrosion potentials of uncoupled and galvanically coupled alloy 825/A516 steel specimens in air-saturated 1,000 ppm Cl^- solutions at 95 °C. Galvanically coupled test specimens were connected through mill scale on A516 steel surface and passive oxide on the alloy 825 surface.

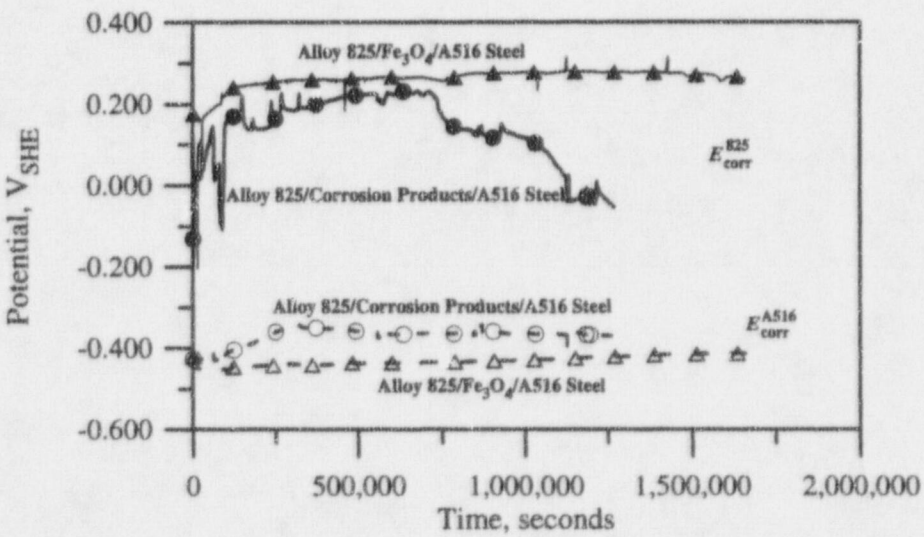

Figure 3-15. Corrosion potentials of galvanically coupled alloy 825/A516 steel specimens in air-saturated 1,000 ppm Cl^- solutions at 95 °C. A516 specimens were covered with a mill scale and the alloy 825 specimens were passivated. Specimens were separated by a 1.5-mm-thick O-ring filled with either corrosion products or Fe_3O_4.

4 DISCUSSION

Although increases in temperature decrease E_{corr}^{825}, the E_{couple} of the alloy 825/A516 steel couple is raised slightly. This is the result of the rise in E_{corr}^{steel} due to increases in both the limiting current density for O_2 reduction and the dissolution kinetics of the steel. The most important effect of elevation of the temperature, as shown in figure 3-2a, is the substantial decline of E_{rp}. In addition, significant changes in the chemical composition of the solution contacting the WP surface can be expected at high temperatures as a result of water evaporation. In the emplacement drift, water is first presumed to contact the WPs when the temperature is close to the boiling point and the RH at the WP surface exceeds the critical RH necessary to stabilize a water film of sufficient thickness on the metal surface able to sustain electrochemical reactions. The time necessary to penetrate the outer CAM must be considered to determine the temperature of the WP when galvanic corrosion begins. The temperature ranges given in figure 3-2a represent the bounding values of the WP temperatures that can be expected at the time galvanic corrosion is initiated. Fast penetration of the outer containment barrier will result in galvanic corrosion starting at temperatures close to 368 K. If penetration of the outer barrier takes many thousands of years, then the WP temperatures will have substantially decreased and the likelihood of localized corrosion of the inner barrier will be reduced. The main effect of temperature is the required increase in η from approximately 0.2 to 0.4 to avoid localized corrosion of alloy 825 when the temperature at which galvanic coupling occurs is raised from 273 to 368 K.

The effect of pH is depicted in figures 3-4 through 3-6. As already noted, groundwater contacting the containers is expected to be alkaline (pH $\geq$ 9). The effect of temperature on the HCO_3^-/CO_3^{2-} concentration ratio, as a consequence of the removal of CO_2 from the solution, will cause the pH to increase. In addition, interactions with the concrete used to construct the underground facilities will increase the pH of the groundwater. The most important effect of the elevated pH is the passivation of the A516 steel overpack (Uhlig and Revie, 1985). The purpose of the outer overpack is to provide a corrosion allowance barrier that will corrode in a uniform and predictable manner. As long as the outer overpack is intact, the thickness of this barrier will act as a gamma radiation shield preventing radiolysis of the groundwater and subsequent formation of highly oxidizing species such as H_2O_2. Failure of the WP by uniform corrosion will take several thousands of years. The extended time for the failure of the outer barrier is a design feature of the WP and will allow a significant period for the radioactive decay of the waste. As a result, when the inner barrier is exposed after the failure of the outer barrier by uniform corrosion, radiolysis of the groundwater will no longer occur and the temperature of the WP will be substantially reduced.

As previously noted, passivation of the A516 steel overpack occurs if the pH is above 9, leading to a decrease in the uniform corrosion rate of the overpack. When passivated, however, carbon steels become susceptible to localized corrosion in chloride-containing solutions. Marsh, et. al. (1986) reported pitting of steel in simulated groundwater of pH 9.2 containing 0.001 M HCO_3^-/CO_3^{2-} in the presence of 10 ppm Cl^- at 50 °C (323 K). A similar or even more aggressive environment in terms of Cl^- concentration and temperature can be expected to contact the WP emplaced in a repository located in the unsaturated zone. If initiated, penetration of the A516 steel overpack by localized corrosion will occur much faster than failure by uniform corrosion. Figure 3-5 shows the calculated $E_{corr}^{825,WP}$ and the E_{rp} of alloy 825 measured in a 1,000 ppm Cl^- solution. A substantially different environment exists inside localized corrosion enclaves independent of the bulk environment. The environment inside pits is known to be enriched in H^+ ions as a result of the hydrolysis of Fe^{2+} cations and contains a high concentration of Cl^- ions to maintain electroneutrality. After pits penetrate through the outer barrier, the inner barrier will then be exposed to the aggressive pit

electrolyte. As previously indicated, the E_{rp} of the corrosion-resistant barrier is strongly dependent on Cl^- concentration. The end result of the high pH in the near-field environment is a reduction in the uniform corrosion rate of the A516 steel barrier due to passivity, accompanied by the initiation and growth of pits that generate a localized environment in which alloy 825 is prone to localized corrosion. This is evident in figure 3-12 where the corrosion potential of the galvanic couple is strongly dependent on pH. In alkaline 1,000 ppm Cl^- solutions, the corrosion potential is higher and has significantly more variation that the corrosion potential of a galvanic couple in a neutral or acidic chloride solution. These variations are likely caused by repeated breakdown and repassivation events on the A516 steel surface. When passive, the dissolution kinetics are altered. Under active conditions the Tafel slope for dissolution has been measured to be 40 mV/decade. Under passive conditions, the slope of the potential versus logarithm of current curves would increase and the corrosion potential would be pushed to higher values. The main effect of the lower pH in the pit environment is the need of a more efficient galvanic couple to avoid localized corrosion of alloy 825 because the threshold value for η increases from 0.3 to 0.45 with a pH decrease from 7 to 3, as noted in figure 3-5a.

As shown in figure 3-7, the main effect of decreasing the p_{O_2} is the reduction in $E_{corr}^{825,WP}$. A substantial decrease in the E_{corr}^{steel} is also expected for A516 steel in an alkaline environment in which passive conditions prevail. Pitting corrosion, however, may occur even in partially deaerated environments due to the very low values of E_p and E_{rp} for A516 steel in Cl^- solutions (Cragnolino et al., 1998). Nevertheless, passivity of A516 steel may not be sustained in a fully deaerated environment and, hence, the high aspect ratio characteristic of a pit cannot be maintained. Pits will tend to spread laterally and coalesce together, leading to less-localized, nonuniform corrosion. This form of corrosion can also occur if the pH of the near-field environment is lower than 9. This is the morphology of the attack, although not defined in relation to the pH, assumed in the aqueous corrosion model for carbon steel adopted in TSPA-95 (TRW Environmental Safety Systems, Inc., 1995).

Since the passive dissolution rate for alloy 825 is independent of the concentration of oxygen, C_{O_2}, reducing the $E_{corr}^{825,WP}$ below the E_{rp} for all values of η requires that the diffusion limiting current for the reduction of oxygen be less than the passive current density of alloy 825. This condition is fulfilled when the p_{O_2} is 2.7×10^{-4} atm for a i_{pass}^{825} of 10^{-3} A/m^2. As presented in figure 3-8a, no localized corrosion of alloy 825 can occur under these conditions even in the absence of galvanic coupling ($\eta = 0$) since the $E_{corr}^{825,WP}$ is always lower than E_{rp}. In the case of steel (see figure 3-7), the rising cathodic current with increasing limiting current for O_2 reduction is balanced by an increase in the I_{corr}^{steel}, resulting in a reduced lifetime for the outer overpack. Figure 3-8a shows localized corrosion of alloy 825 in air-saturated solutions is avoided when $\eta > 0.4$, whereas E_{rp} is not reached in deaerated solutions even in the absence of galvanic coupling ($\eta = 0$). Under deaerated conditions, the lifetime of both the A516 steel overpack and the CRM inner barrier will be significantly extended. The lifetimes of Ti based alloys as well as Cu alloys, considered as possible container materials for the disposal of SF in Canada, have also been reported to be strongly influenced by the amount of available O_2 in the repository (King and Kolar, 1996; Shoesmith et al., 1996). In the Canadian program, complete consumption of the available O_2 is expected to occur in a few hundred years as a result of partial oxidation of the containers when emplaced in a sealed repository located in deep, water-saturated geologic formations. Afterward, the corrosion rate of the containers is expected to be so low that containment of the waste will be assured for many thousands of years. Significant reductions in the O_2 concentrations in the

proposed YM repository, however, are not expected. As a consequence, corrosion rates of the materials in an air-saturated environment must be considered.

In this investigation, the effect of area ratio on the $E_{corr}^{825,WP}$ and the $E_{corr}^{steel,WP}$ was found to be minimal, as presented in figure 3-10. Even with a 12.5:1 area ratio of alloy 825 to A516 steel, the dissolution of the steel decreases the $E_{corr}^{825,WP}$ below the E_{rp} for $\eta > 0.3$. The area ratio, however, has a pronounced effect on the dissolution rate of carbon steel. Figure 4-1 shows the i_{steel} for a 1 m^2 area of steel with three values for the area ratio. An increase in i_{steel} from 0.8 to 10 A/m^2 is predicted as a result of the elevation in alloy 825 to A516 steel area ratio from 0.025:1 to 12.5:1. For an area ratio equal to 1, the current density is 1.3 A/m^2. It should be noted for comparison that Zamani et al., (1986) measured the corrosion current density in seawater to be in the range of 0.3 to 0.7 A/m^2 for a carbon steel/SS couple with a 1:1 area ratio. The results indicate that, as long as a small amount of A516 steel is coupled to the alloy 825 inner overpack, galvanic protection of the alloy 825 barrier should occur. These calculations do not consider the effect of potential and current density distributions. When a low resistivity electrolyte is between the barrier layers, then the effect of potential and current density distributions are negligible. Significant variations of the potential and current density distributions may be present after much of the A516 steel overpack has corroded away. The DOE model of WP performance considers that galvanic protection of the inner barrier will occur until 75 percent of the outer barrier has corroded (TRW Environmental Safety Systems, Inc., 1995). Although no justification is provided for the 75 percent criteria, results of previous modeling efforts of galvanic corrosion and cathodic protection systems, where the potential and current density distributions were calculated, suggest there should be a minimum amount of A516 steel necessary to galvanically protect the inner corrosion resistant barrier.

By far the dominant factor in determining $E_{corr}^{825,WP}$ is the value of η as a result of the assumed relationship between parameters discussed in previous subsections. Because of the active behavior of steel, the value of η is not so significant in determining $E_{corr}^{steel,WP}$. As indicated by the calculations, the highest resistance that would yield the minimum value of η required to avoid the occurrence of localized corrosion for alloy 825 is typically smaller than 500 ohms.

In addition to the electrolyte, oxide films and corrosion products could be present between the inner and outer container barriers. Therefore, the contribution of resistances of the oxides and corrosion products should be discussed. Wilhelm (1988) investigated the electronic properties of different oxides and their effect on galvanic corrosion. In Wilhelm's study, oxides were classified as insulators, conductors, n-type semiconductors, and p-type semiconductors based on the band gap between the conduction and valance bands. The p-type oxides include NiO. These oxides can support the reduction of O_2 and H^+ ions, but may also be reduced. Iron oxides such as Fe_2O_3 are n-type semiconductors (the oxide is deficient in oxygen) and can readily support the reduction of O_2 or H^+ ions. As a result, materials coated with n-type oxides are at risk for localized attack. Wilhelm (1988) did not investigate corrosion products such as FeOOH. Materials coated with insulator oxides such as Al_2O_3 or ZrO_2 can be subject to localized attack but only if electron conduction by tunneling occurs through a thin oxide layer.

The interface between the A516 steel overpack and the alloy 825 inner barrier may consist of Fe_2O_3, Fe_3O_4, corrosion products containing Fe^{2+} and Fe^{3+}, Cr_2O_3, and a solution between the materials. The resistance of the interface is determined by the resistances of these layers. The Cr_2O_3, which is expected to form on the

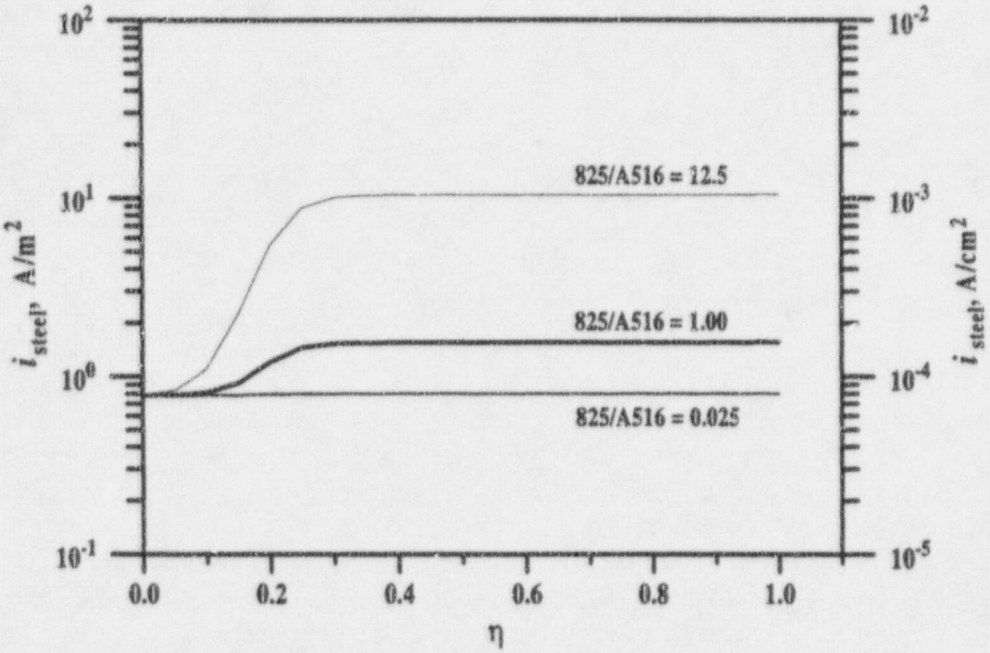

Figure 4-1. Effect of area ratio of the alloy 825/A516 steel bimetallic couple on the dissolution current density of A516 steel as a function of η in an air saturated solution of pH 5 at 368 K (95 °C).

alloy 825 surface, is an electronic conductive oxide that facilitates electron transfer for the cathodic reduction of O_2 and H_2O. From the resistance values shown in table 3-2, it is apparent that the oxides formed on alloy 825 are indeed quite conductive. For A516 steel, a slight increase in resistance was observed after oxidation at 250 °C. The mill scale formed on the A516 steel surface has a very high resistance. In addition, corrosion products such as Fe_3O_4, and γ-FeOOH all have a high resistance. The porosity of the corrosion products and the mill scale is apparently quite high and conduction is dominated by the electrolyte present in the pores. The resistance of $FeCl_2 \cdot 4H_2O$ with a 1,000 ppm Cl^- solution is approximately 70 ohms. As a result of the high solubility of $FeCl_2 \cdot 4H_2O$, a near saturated chloride solution would be present between the A516 steel surfaces. Under these conditions, which are expected to occur if a pit penetrated the outer A516 steel barrier, the low resistivity of the phases present at the interface suggests the value of η can be expected to be close to 1.0. Under these conditions, the galvanic corrosion potentials of the container materials will be reduced to low values because of the dominating effect of the iron dissolution kinetics. Localized corrosion of alloy 825 will be prevented until significant loss of the steel corrosion allowance barrier has occurred and large potential and current density distributions are present. More sophisticated techniques such as the boundary element method will be required to model such potential and current density distributions.

The formation of an oxide on alloy 825 and the presence of a mill scale on A516 steel had only a marginal effect on the efficiency of the galvanic couple. Corrosion potentials of A516 steel and either thermally oxidized or passivated alloy 825 differed by as much as 200 mV in the early stages of exposure. The decrease in the corrosion potential of alloy 825 indicated that the efficiency of the galvanic couple actually increased. This behavior is likely to be a result of the removal of much of the mill scale, after active corrosion of the A516 steel, by being immersed in an acidic chloride solution.

The formation of a solution saturated corrosion product layer between the A516 steel and alloy 825 barriers was found to be quite detrimental to the galvanic coupling of the WP materials. The corrosion potential of alloy 825 was 500 to 600 mV greater than the corrosion potential of A516 steel. Reagent grade Fe_3O_4 and Fe_2O_3 were found to provide a more resistive path to the flow of galvanic current than A516 steel corrosion products. The corrosion potentials of the polished and passivated alloy 825 specimens were over 0.200 V_{SHE}. Previous investigations have shown that the initiation of localized corrosion on alloy can occur if the corrosion potential of the material exceeds the repassivation potential. For the 1,000 ppm Cl^- solution used in this study, the repassivation potential has been measured to be in the range of 0.250 to 0.350 V_{SHE}. When corrosion products were placed between the specimens, the corrosion potential of the alloy 825 specimen started to decrease after approximately 6 days. For this case, localized corrosion of alloy 825 is not expected to occur since the corrosion potential is more than 200 mV below the repassivation potential. With Fe_3O_4, between the barrier materials, the corrosion potential of alloy 825 was above the repassivation potential and therefore vulnerable to localized corrosion.

From the data presented in table 3-1, it is apparent that the calculated corrosion potentials of the galvanic couples are lower than the measured corrosion potentials. In addition, the uncoupled corrosion potential for alloy 825 is considerably less than the calculated corrosion potential for this material. For the case of alloy 825, however, the calculated corrosion potential is several hundred millivolts above the repassivation potential. Previous investigations have indicated that localized corrosion is quickly initiated under these conditions (Sridhar et al., 1995). As a result, the corrosion potential would not be expected to be maintained hundreds of millivolts above the repassivation potential since the active dissolution of the material during localized corrosion would reduce the corrosion potential.

The corrosion potential of uncoupled A516 steel (figure 3-14) tended to increase with time from an initial value of -0.450 V_{SHE} to a maximum of -0.350 V_{SHE} toward the end of the test. Under these conditions the formation of a stable passive film impeding the dissolution of A516 steel will not occur (Pourbaix, 1974). In addition, the kinetics of the oxygen reduction are not expected to vary with exposure time. The concentration of Fe^{2+} may vary with exposure time as the A516 steel specimen corrodes. Work by Tremaine and LeBlanc, (1980) suggests that at pH 5 the equilibrium Fe^{2+} concentration is approximately 7×10^{-6} molar. At pH 3, this increases to 5×10^{-4} molar. Increased Fe^{2+} concentration can be expected to increase the corrosion potential of A516 steel. Figure 4-2 shows a portion of an Evans diagram with the kinetics of A516 steel dissolution calculated as a function of Fe^{2+} concentration. The corrosion potential of A516 steel is the potential defined by the intersection of the total cathodic reduction curve (i.e., $H_2O + O_2$ reduction) with the A516 steel dissolution curve. It is apparent that an order of magnitude increase in the Fe^{2+} concentration increases the corrosion potential of A516 by 30 mV. Calculation of the corrosion potential of A516 and galvanic corrosion potentials of the A516/alloy 825 couples listed in table 3-1 were performed using a Fe^{2+} concentration of 10^{-6} molar. From figure 4-2, it is apparent that the calculated corrosion potential of A516 steel would be elevated by as much as 75 mV with higher concentrations of Fe^{2+} in solution.

The effect of higher Fe^{2+} concentrations on the galvanic corrosion potentials is shown in figure 4-3. Under perfect galvanic coupling conditions, the galvanic corrosion potential is largely dictated by the corrosion potential of A516 steel. Since the corrosion potential of A516 steel is elevated by 60 mV when the Fe^{2+} concentration is increased from 10^{-6} to 10^{-4} molar, the galvanic corrosion potential is also increased. While increases in the Fe^{2+} concentration cannot entirely account for the differences in the calculated and measured galvanic corrosion potentials, it is apparent that the Fe^{2+} concentration may increase by over 2 orders of magnitude as the solution pH is decreased from 7 to 3 and, as a result, the calculated corrosion potentials and galvanic corrosion potentials would increase.

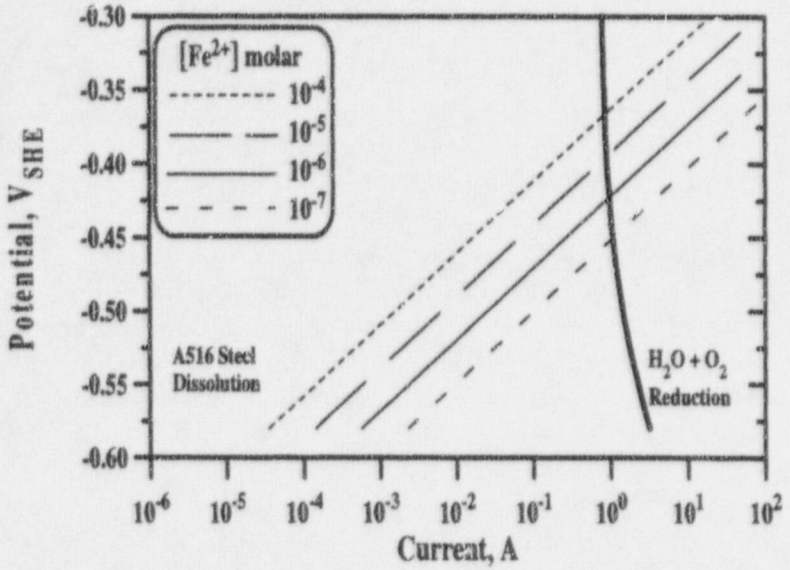

Figure 4-2. Evans diagram showing the effect of Fe^{2+} concentration (10^{-7} to 10^{-4} molar) on the calculated anodic dissolution kinetics and corrosion potential of A516 steel in a pH 3 solution at 368 K (95 °C).

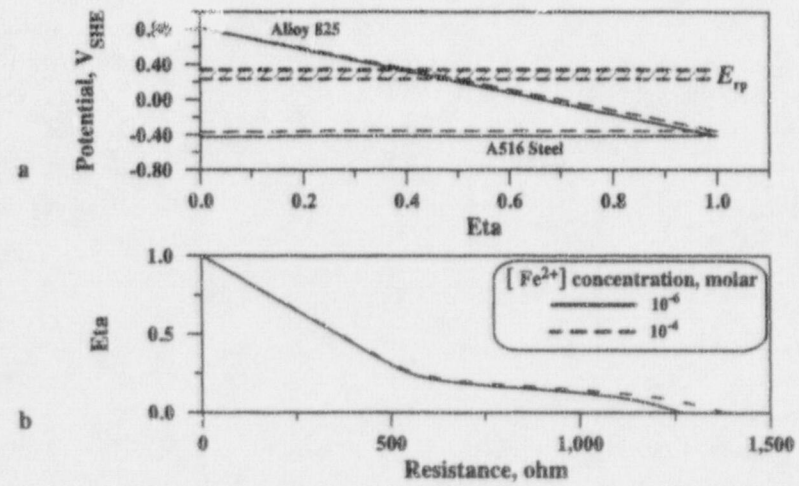

Figure 4-3. (a) Plot of the calculated galvanic corrosion potentials of alloy 825 and A516 steel as a function of the efficiency of the galvanic coupling, η, at pH 3 and two values of Fe^{2+} concentration (10^{-6} and 10^{-4} molar). Values of the repassivation potential, E_{rp}, of alloy 825 in 1,000 ppm chloride solutions at 368 K (95 °C) are included. (b) Value of η as a function of the resistance of the galvanic couple for two Fe^{2+} concentrations.

5 CONCLUSIONS

Calculations of the galvanic corrosion potentials indicate that the temperature and the partial pressure of oxygen are the most significant environmental parameters in determining the lifetime of the WP. Although changes in temperature do not have a significant effect on the galvanic corrosion potentials of the container materials, the repassivation potential, which is conservatively chosen as the critical potential for the initiation of localized corrosion on alloy 825, decreases significantly with increasing temperature. As a result, alloy 825 becomes less susceptible to localized corrosion at lower temperatures. On the other hand, significant decreases in the galvanic corrosion potentials are calculated as the partial pressure of oxygen is reduced. The corrosion rate of A516 steel was decreased by over an order of magnitude when the environment was fully deaerated. A significant decline in the galvanic corrosion potential of alloy 825 is also estimated. As a consequence, for partial pressures of oxygen less than 2.7×10^{-4} atm, alloy 825 can be protected against localized corrosion even in the absence of galvanic coupling to A516 steel. Variations in the area ratio of alloy 825 to A516 steel have only a minimal influence on the galvanic corrosion potentials and do not modify the value of the galvanic coupling efficiency required to avoid the occurrence of localized corrosion of alloy 825. The results of galvanic corrosion tests are in agreement with the calculated values of the galvanic corrosion potentials when the barrier materials are perfectly coupled. Nevertheless, the study of other geometries, covering a wide range of pit distributions and pit sizes, needs to be performed to attain a more complete understanding of the influence of the effective area ratio between both container materials.

An analysis of the resistance of the galvanic couple between alloy 825 and A516 steel is also performed for the pit geometry considered in this study. The analysis suggests that galvanic protection of the inner barrier by the perforated A516 steel overpack can be accomplished if a good metallic contact exists between both barriers. Therefore, localized corrosion of the alloy 825 inner container can be avoided by galvanic coupling to the outer container if the resistance of the couple is lower than 500 ohms. On the basis of literature information and resistance measurements, it appears the oxide films on the materials and the solution in contact with the barrier layers have a relatively low resistance, suggesting that a conductive path for the flow of galvanic current exists. Galvanic protection of the inner alloy 825 barrier can be achieved unless electronic conduction is affected by the lack of metallic contact between the barriers.

A methodology for estimating the galvanic coupling efficiency from the resistance of the galvanic couple is developed. Considering only the resistance of the electrolyte solution, the value of the galvanic coupling efficiency is estimated to range from 0.97 with a low conductivity solution to more than 0.99 with a high conductivity solution. Oxides formed on Cr-containing corrosion-resistant alloys are good conductors. As a result, the presence of a Cr oxide on an inner barrier constructed of an alloy such as alloys 825, 625, or C-22 will not significantly reduce the galvanic coupling efficiency. The semiconductive nature of the oxides formed on A516 steel should also provide a conductive path that will not significantly impede the flow of galvanic current. It was found that the presence of nonconductive scales and corrosion products increases the resistance and limits the efficiency of the galvanic coupling. However, the conductivity of the solution present in the pores of these phases is critical to maintaining a low resistance path between the barrier layers.

From this investigation it may be concluded that failure of the outer A516 steel corrosion allowance barrier by localized corrosion will result in galvanic protection of the inner corrosion resistant barrier. Since the efficiency of the galvanic couple is not strongly dependent on either the environmental variations or area ratio of the galvanic contact, complete protection of the inner corrosion resistant barrier from localized corrosion can be expected. Oxide scales and corrosion product layers between the barrier materials were observed to reduce the galvanic coupling efficiency. However, sufficient galvanic coupling was retained such

that the corrosion potential of alloy 825 was continuously maintained below the repassivation potential for localized corrosion.

There are several limitations to the simplified calculations presented in this report. The electrochemical reactions considered in this investigation are limited to the dissolution of the metals and the reduction of both O_2 and H_2O. While these are the primary corrosion reactions, the corrosion kinetics may be significantly accelerated by the presence of a highly oxidizing species such as H_2O_2 (the main radiolytic product) or Fe^{3+} ions (which can be produced by the oxidation of Fe^{2+} species in solution by the available O_2). At present, formation of these species within the repository has not been conclusively determined but it is expected that, after thousands of years, gamma radiolysis will decrease sufficiently to make the generation of H_2O_2 negligible. The thickness of the inner overpack is such that alpha radiolysis can be neglected at its outer surface. Yet another limitation in the present analysis is the lack of knowledge regarding the near-field environmental conditions. These conditions will be strongly dependent on the design and thermal loading strategy for the proposed repository. The time-dependent variation of temperature, partial pressure of oxygen, chemistry of the water contacting the containers, and other environmental variables can have a significant impact on the time that galvanic protection of the inner barrier will be maintained and therefore, on container lifetimes. A third limitation is the lack of an appropriate estimate of the wetted area of the A516 steel overpack. A more accurate assessment of the near-field environment and information on the final WP detailed design are important to better define the conditions and configuration of the system under study.

6 REFERENCES

Atkins, J.E., and J.H. Lee. 1996. *User's Guide to Waste Package Degradation (WAPDEG) Simulation Code*. Version 1.0. Preliminary draft. Las Vegas, NV: INTERA, Inc.

Bockris, J.O'M., and A.K.N. Reddy. 1977. *Modern Electrochemistry*. New York: Plenum Press.

Bockris, J.O'M., D. Drazic, and A.R. Despic. 1961. The electrode kinetics of the deposition and dissolution of iron. *Electrochimica Acta* 4: 325–361.

Calvo, E.J. 1979. *Study of the Electroreduction Reaction of Oxygen on Passive Metals in Different Aqueous Media* (in Spanish). Ph.D. dissertation, Universidad Nacional de La Plata (Argentina).

Calvo, E.J., and D.J. Schiffrin. 1988. The electrochemical reduction of oxygen on passive iron in alkaline solutions. *Journal of Electroanalytical Chemistry* 243: 171–185.

Conway, B.E. 1952. *Electrochemical Data*. Amsterdam, Netherlands: Elsevier.

Cragnolino, G.A., D.S. Dunn, P. Angell, Y-M. Pan, and N. Sridhar. 1998. Factors influencing the performance of carbon steel overpacks in the proposed high-level nuclear waste repository. *CORROSION/98*. Paper No. 147. Houston, TX: NACE International.

Dunn, D.S., and G.A. Cragnolino. 1997. *An Analysis of Galvanic Coupling Effects on the Performance of High-Level Nuclear Waste Container Materials*. CNWRA 97-010. San Antonio, TX: Center for Nuclear Waste Regulatory Analyses.

Dunn, D.S., G.A. Cragnolino, and N. Sridhar. 1997. *An Electrochemical Approach to Predicting Long-Term Localized Corrosion of Corrosion Resistant Container Materials*. San Antonio, TX: Center for Nuclear Waste Regulatory Analyses.

Heusler, K.E. 1976. Influence of temperature and pressure on the kinetics of electrode processes. *High Temperature, High Pressure Electrochemistry in Aqueous Systems*. R.W. Staehle, D. deG. Jones, and J.E. Slater, eds. Houston, TX: National Association of Corrosion Engineers: 387-399.

King, F., and M. Kolar. 1996. A numerical model for the corrosion of copper nuclear fuel waste containers. *Scientific Basis for Nuclear Waste Management XIX*. W.M. Murphy and D.A. Knecht, eds. Pittsburgh, PA: Materials Research Society: Symposium Proceedings 412: 555–562.

Laycock, N.J, J. Stewart, and R.C. Newman. 1997. The initiation of crevice corrosion in stainless steels. *Corrosion Science* 39: 1791–1809.

Macdonald, D.D., and M. Urquidi-Macdonald. 1990. Thin-layer mixed-potential model for the corrosion of high-level nuclear waste canisters. *Corrosion* 46: 380–390.

Marsh, G.P., K.J. Taylor, I.D. Bland, C. Wescott, P.W. Tasker, and S.M. Sharland. 1986. Evaluation of the localized corrosion of carbon steel overpacks for nuclear waste disposal in granite environments. *Scientific Basis for Nuclear Waste Management IX*. L.W. Werme, ed. Pittsburgh, PA: Materials Research Society: Symposium Proceedings 50: 421–428.

Mohanty, S., G.A. Cragnolino, T. Ahn, D.S. Dunn, P.C. Lichtner, R.D. Manteufel, and N. Sridhar. 1997. *Engineered Barrier System Performance Assessment Code: EBSPAC Version 1.1 Technical Description and User's Manual*. CNWRA 97-006. San Antonio, TX: Center for Nuclear Waste Regulatory Analyses.

Morgan, J. 1993. *Cathodic Protection*. 2nd Edition. Houston, TX: NACE International.

Pourbaix, M. 1974. *Atlas of Electrochemical Equilibria in Aqueous Solutions*. Houston, TX: National Association of Corrosion Engineers.

Roy, A.K., D.L. Fleming, and S.R. Gorton. 1996a. Effect of chloride concentration and pH on pitting corrosion of waste package container materials. Paper 182. *190th Electrochemical Society Meeting*. Pennington, NJ: The Electrochemical Society.

Roy, A.K., D.A. Jones, and R.D. McCright. 1996b. *Degradation Mode Survey. Galvanic Corrosion of Candidate Metallic Materials for High-Level Radioactive Waste Disposal Containers*. UCRL-ID-125645. Livermore, CA: Lawrence Livermore National Laboratory.

Scully, J.R., and H.P. Hack. 1984. Galvanic corrosion predicting using long- and short-term polarization curves. *CORROSION/84*. Paper no 34., Houston, TX: NACE International.

Shoesmith, D.W., F. King, and B.M. Ikeda. 1996. The indefinite containment of nuclear fuel wastes. *Scientific Basis for Nuclear Waste Management XIX*. W.M. Murphy and D.A. Knecht, eds. Pittsburgh, PA: Materials Research Society: Symposium Proceedings 412: 563–570.

Sridhar, N., G.A. Cragnolino, D.S. Dunn, and H.K. Manaktala. 1994. *Review of Degradation Modes of Alternate Container Designs and Materials*. CNWRA 94-010. San Antonio, TX: Center for Nuclear Waste Regulatory Analyses.

Sridhar, N., G.A. Cragnolino, and D.S. Dunn. 1995. *Experimental Investigations of Failure Processes of High-Level Radioactive Waste Container Materials*. CNWRA 95-010. San Antonio, TX: Center for Nuclear Waste Regulatory Analyses.

Tremaine, P.R., and J.C. LeBlanc. 1980. The solubility of magnetite and hydrolysis and oxidation of Fe^{2+} in water to 300 °C. *Journal of Solution Chemistry* 9(6): 415–442.

TRW Environmental Safety Systems, Inc. 1995. *Total System Performance Assessment—1995: An Evaluation of the Potential Yucca Mountain Repository*. B00000000-01717-2200-00136. Las Vegas, NV: TRW Environmental Safety Systems, Inc.

TRW Environmental Safety Systems, Inc. 1996. *Mined Geologic Disposal System Advanced Conceptual Design Report. Engineered Barrier Segment/Waste Package.* B00000000-01717-5705-00027. Las Vegas, NV: TRW Environmental Safety Systems, Inc.

Uhlig, H.H., and R.W. Revie. 1985. *Corrosion and Corrosion Control.* New York: John Wiley and Sons.

U. S. Department of Energy. 1997. *Site Characterization Progress Report: Yucca Mountain, Nevada. October 1, 1996 - March 31, 1997.* Number 16. Washington, DC: U.S. Department of Energy.

Wilhelm, S.M., 1988. Galvanic corrosion caused by corrosion products. H.P. Hack, ed. ASTM STP 978. *Galvanic Corrosion.* Philadelphia, PA: 23–34.

Zamani, N.G., J.F. Porter, and A.A. Mufti. 1986. A survey of computational efforts in the field of corrosion engineering. *International Journal for Numerical Methods in Engineering* 23: 1,295–1,311.